

# Weathering, sedimentary and diagenetic controls of mineral and geochemical characteristics of the vertebrate-bearing Silesian Keuper

J. ŚRODON<sup>1,\*</sup>, J. SZULC<sup>2</sup>, A. ANCKIEWICZ<sup>1</sup>, K. JEWUŁA<sup>1,3</sup>, M. BANAS<sup>1</sup>  
AND L. MARYNOWSKI<sup>4</sup>

<sup>1</sup> Institute of Geological Sciences, Polish Academy of Sciences – Research Centre in Kraków, ul. Senacka 1, 31-002 Kraków, Poland, <sup>2</sup> Jagiellonian University, Institute of Geological Sciences, Oleandry 2a, 30-063 Kraków, Poland, <sup>3</sup> Chemostrat Ltd, Unit 1 Ravenscroft Court, Buttingcross Ind. Estate, Welshpool, Powys, SY21 8SL, UK, and <sup>4</sup> Faculty of Earth Sciences, University of Silesia, Będzińska 60, 41-200 Sosnowiec, Poland

(Received 24 April 2014; revised 17 August 2014; Editor: George Christidis)

**ABSTRACT:** Mudstones and claystones from the southern marginal area of the European Upper Triassic, midcontinental Keuper basin (Silesia, southern Poland) were investigated using XRD, organic and inorganic geochemistry, SEM, K-Ar of illite-smectite, AFT, and stable isotopes of O and C in carbonates in order to unravel the consequent phases of the geological history of these rocks, known for abundant fossils of land vertebrates, and in particular to evaluate the diagenetic overprint on the mineral composition. The detected and quantified mineral assemblage consists of quartz, calcite, dolomite, Ca-dolomite, illite, mixed-layer illite-smectite, and kaolinite as major components, plus feldspars, hematite, pyrite, chlorite, anatase, siderite, goethite as minor components. Palygorskite, gypsum, jarosite and apatite were identified in places.

The K-Ar dates document a post-sedimentary thermal event, 164 Ma or younger, which resulted in partial illitization of smectite and kaolinite. The maximum palaeotemperatures were estimated from illite-smectite as ~125°C. Apatite fission track data support this conclusion, indicating a 200–160 Ma age range of the maximum temperatures close to 120°C, followed by a prolonged period of elevated temperatures. These conclusions agree well with the available data on the Mesozoic thermal event, which yielded Pb-Zn deposits in the area. Organic maturity indicators suggest the maximum palaeotemperatures <110°C.

Palygorskite was identified as authigenic by crystal morphology (TEM), and calcite by its accumulation in soil layers and by its isotopic composition evolving with time, in accordance with the sedimentary and/or climatic changes. Dolomite isotopic composition indicates more saline (concentrated) waters. Palygorskite signals a rapid local change of sedimentary conditions, correlated with algal blooms. This assemblage of authigenic minerals indicates an arid climate and the location at the transition from a distal alluvial fan to mudflat.

Fe-rich smectite, kaolinite, and hematite were products of chemical weathering on the surrounding lands and are therefore mostly detrital components of the investigated rocks. Kaolinite crystal morphology and ordering indicates a short transport distance. Hematite also crystallized *in situ*, in the soil horizons. A large variation in kaolinite/2:1 minerals ratio reflects hydraulic sorting, except of the

\* E-mail: ndsrodon@cyf-kr.edu.pl  
DOI: 10.1180/claymin.2014.049.4.07

Rhaetian, where it probably signals a climatic change, i.e. a shift in the weathering pattern towards kaolinite, correlated with the disappearance of hematite. Quartz, 2M<sub>1</sub> illite, and minor feldspars and Mg-chlorite were interpreted as detrital minerals. The documented sedimentation pattern indicates that in more central parts of the Keuper playa system, where an intense authigenesis of the trioctahedral clays (chlorite, swelling chlorite, corrensite, sepiolite) took place, illite and smectite were the dominant detrital clay minerals.

Cr/Nb and Cr/Ti ratios were found as the best chemostratigraphic tools, allowing for the correlation of all investigated profiles. A stable decrease of these ratios up the investigated sedimentary sequence is interpreted as reflecting changes in the provenance pattern from more basic to more acidic rocks.

**KEYWORDS:** AFT, carbonate stable isotopes, chemostratigraphy, clay minerals, diagenesis, hematite, K-Ar, Keuper, palygorskite, playa, provenance, quantitative XRD, weathering.

The Silesian Keuper pertains to the southern marginal area of the Upper Triassic Keuper intracontinental basin, with the depocentre extending from central Poland towards Germany, England, and the southern part of the North Sea (Fig. 1). The Silesian Keuper has generated a lot of interest recently after discoveries of abundant fossils of land vertebrates, and in particular *Dinosauromorpha* (Dzik *et al.*, 2000).

The European Keuper basin is one of the classic areas for the investigation of clay autigenesis in sedimentary environments of the arid zone. The clay studies were initiated by Endell in the thirties of 20th century and have continued, mostly in Germany, France, Great Britain, and Spain until recently (reviews in Krum, 1969, and Jeans, 2006). Corrensite, the most common trioctahedral regular mixed-layer clay mineral, was first identified in a Lower Triassic marl (Lippman, 1956) and was named after a prominent early investigator of the Triassic clays.

The provenance studies (K-Ar of micas: Paul *et al.*, 2008) indicate that the Keuper basin was supplied by detrital material from several surrounding elevated areas. As summarized by Krum (1969), close to the basin margins the detrital assemblage: kaolinite, illite, and minor Fe-chlorite have been recorded in Scandinavia, Central Europe and North Africa. Smectites or illite-smectites and illite occur in the entire basin, while Mg-rich clays such as chlorite, swelling chlorite, corrensite, sepiolite, and palygorskite are present mostly in the central part. Both sepiolite and palygorskite occur as widespread thin layers, most often within the broader zones of the Mg-chloritic minerals. Massive occurrences of 1M or 1Md ferruginous illite were recognized in several areas and interpreted as pedogenic (Jeans *et al.*, 1994). The Mg-clays have been recognized at an

early stage as authigenic, but their more detailed origin (transformation *vs.* neof ormation, low or high temperature) is still a matter of debate (Jeans, 2006).

Most Keuper studies lack maximum palaeotemperature measurements, which are necessary to evaluate the degree of diagenetic overprint on the pattern resulting from the weathering and sedimentary processes. Jeans *et al.* (2005) made such a study using a spore colour index and concluded that corrensites and Mg-chlorites crystallized below 100°C. The origin of illite-smectite remains uncertain.

In this contribution, dealing with the Silesian Keuper, the emphasis is put on a precise evaluation of the diagenetic overprint in order to identify the weathering and sedimentary controls of the mineralogical and geochemical composition of the rocks which are useful for correlation purposes and for the reconstruction of the environment where the dinosaurs have lived. It was hoped also that the application of more accurate quantitative mineralogical techniques should make the genetic interpretations of the clay mineral compositions more reliable, and in particular will permit a distinction of climatic from sedimentary sorting controls over the kaolinite abundance.

The Silesian Keuper sediments are continental and oxidized, consequently with very poor biostratigraphic record; correlations dependant mostly on lithostratigraphy (Szulc & Racki, 2014). For this reason, an attempt was made to correlate the investigated profiles by means of chemostratigraphic tools.

## GEOLOGICAL SETTING

The present day shape of the European Keuper basin is not very different from the original and includes the central playa system surrounded by the

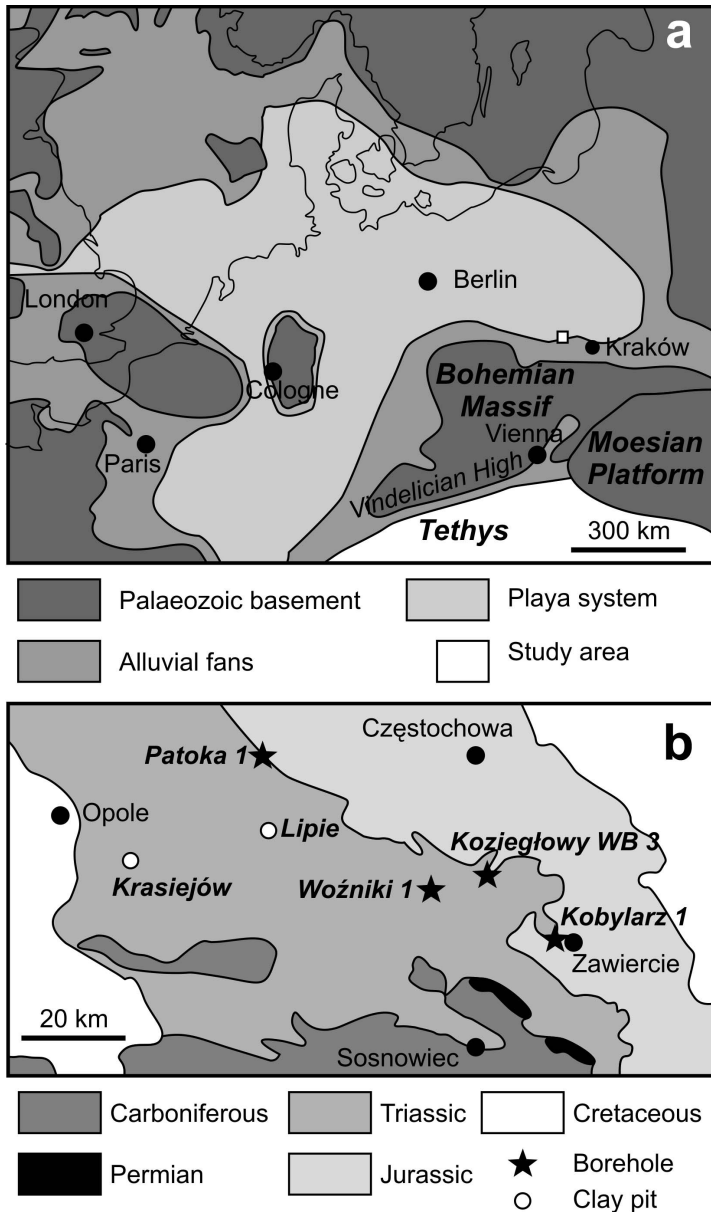


FIG. 1. (a) Palaeogeography of the European Keuper Basin after Ziegler (1990), with the Moesian Platform location after Tari *et al.* (2012), and the study area marked with a rectangle. (b) Location of the studied boreholes and clay pits.

peripheral alluvial fan zone (Fig. 1). The basin developed in an arid subtropical zone, as evidenced by the palaeolatitude ( $\sim 20\text{--}23^\circ\text{N}$ ; *vide* Reinhardt & Ricken, 2000) and by the occurrences of rock salt, gypsum, anhydrite, baryte and celestite (Krum, 1969; Reinhardt & Ricken, 2000; Bzowska &

Racka, 2006; Jeans, 2006). In the south it had connections with the incipient Tethys ocean and some sedimentary events in both basins are concurrent (Feist-Burkhardt *et al.*, 2008).

The Silesian Keuper rocks are mostly red mudstones and claystones, with minor sandstone

and carbonate layers, numerous erosional discontinuities (Deczkowski, 1977), and incipient palaeo-weathering horizons (Szulc, 2005). They are almost flat-lying at the surface, accessible in clay pits and by shallow boreholes. The southern and SW borders of the Silesian Keuper are erosional (Fig. 1), while towards the NE the Triassic rocks dip gently under the Jurassic cover.

The local lithostratigraphic divisions correlate well with the classic divisions in the German part of the basin, so the classic nomenclature will be used. The Keuper succession (in particular its middle and upper parts) displays layer-cake lithostratigraphy, reflecting the general trend from shallow marine to freshwater conditions and climatic fluctuations, ranging between “wetter” and “drier” lithofacies. The main lithostratigraphic units are quite well dated by means of palinostratigraphic data (Orłowska-Zwolińska, 1983; Szulc *et al.*, 2006): Ladinian Grenzdolomite and Carnian Lower Gipskeuper (“dry” intervals: sabkha/playa sediments), followed by Carnian Schilfsandstein fluvial clastic (“wet” interval: braided/anastomosing river sediments), Carnian/Norian Upper Gipskeuper (“dry” interval playa sediments), Norian Steinmergelkeuper (semi-dry to wet facies: ephemeral and/or perennial fluvial sediments), and finally the Rhaetian “wet” facies. Within Steinmergelkeuper locally lacustrine/palustrine carbonates occur (Woźniki Limestone) related to a spring system controlled by a major fault (Szulc *et al.*, 2006). The generally clear and simple stratigraphic pattern is more complex at the level of higher resolution stratigraphy, because of intensive, local syndimentary tectonics and shorter, incidental climatic variations. The most recent lithostratigraphic study (Szulc & Racki, 2014) introduces Grabowa Fm. as the Silesian equivalent of the Upper Gipskeuper plus Steinmergelkeuper intervals.

## MATERIALS AND METHODS

The entire area and the complete profile of the Silesian Keuper were sampled. Samples were collected from four boreholes and two clay pits containing bone beds. The boreholes and the outcrops locations are presented in Fig. 1, while the complete list of investigated samples, along with their sedimentological characteristics is given in Table 1 (Tables 1 & 2 are deposited with the Mineralogical Society and can be found at [http://www.minersoc.org/pages/e\\_journals/](http://www.minersoc.org/pages/e_journals/)

dep\_mat\_cm.html). The complete sedimentological profiles of the studied sites have been published elsewhere (Szulc & Racki, 2014).

In the Woźniki borehole also the underlying Ladinian rocks were sampled and investigated, whereas in the Patoka borehole the overlying Rhaetian sediments were studied. The profiles consist essentially of claystones and mudstones, often with clear indications of weathering and soil-forming processes (nodules, caliche, slickensides, etc.), red, green or variegated in colour. Occasionally carbonate layers and sandstone layers appear. The underlying Ladinian sediments are massive dolomites. The overlying Rhaetian sediments do not have red colours and carbonates, and are more coarse-grained than their Keuper counterparts.

All the samples were crushed to <0.5 mm and separated using a hand splitter into portions for XRD and chemical analyses, following Środoń & Kawiak (2012). Samples for the bulk rock XRD analysis were ground with the ZnO internal standard in the McCrone mill and registered in 2–65°2θ range (Środoń *et al.*, 2001) by Thermo X'tra diffractometer, equipped with Cu tube and the solid-state Peltier-cooled detector. These XRD patterns were then used for the mineral identification, including precise measurements of selected peak positions corrected for the ZnO standard, and the mineral quantification with new QMIN computer program of Marek Szczerba, using natural mono-mineral standards and the approach of Środoń *et al.* (2001).

These data were then used for selecting representative samples for detailed clay mineralogical XRD investigation. The selected samples were treated chemically by the standard procedures to remove carbonates, sulfates, organic matter (OM) and iron oxides (Jackson, 1975) and the <0.2 μm fractions were separated by centrifugation, cleaned of the excess electrolyte, and analysed by XRD in oriented preparations both air-dried and glycolated, with Na as the exchange cation (detailed procedure in Środoń *et al.*, 2006). The smectite content in mixed-layer illite-smectite (%S) was measured using a selected peak positions technique (Środoń, 1981, 1984), newly calibrated on mono-mineral illite-smectite from bentonites (Środoń *et al.*, 2013). %S was then used to evaluate the maximum palaeotemperatures (Środoń, 2007).

All bulk rock samples were analysed chemically after the water loss measurement (100°C for 24 h)

by ICP-OES and ICP-MS for major elements, trace elements, and *REE* (CHEMOSTRAT laboratory in Welshpool, Powys, UK, according to Jarvis & Jarvis, 1992) and for water loss between room temperature and 200°C in the Kraków laboratory of ING PAN (thermobalance: 3 min. ramp heating plus 25 min. at 200°C). In selected samples N, H, S and total C were measured in air-dry state by elemental analyser at the Warsaw laboratory of ING PAN and then were corrected for the water loss. The total organic carbon (TOC) and gas chromatography-mass spectrometry (GC-MS) analysis were determined at the University of Silesia using an Eltra Elemental Analyzer model CS530 and Agilent 6890 Series Gas Chromatograph interfaced to an Agilent 5973 Network Mass Selective Detector and Agilent 7683 Series Injector (Agilent Technologies, Palo Alto, California, USA). More details are provided in Marynowski *et al.* (2012). Another set of selected samples was analysed after drying in 110°C for B (PGNAA, 0.5 ppm det. limit) and Cl (INAA, 0.01% det. limit) by Actlabs (Canada).

The analyses of isotopic composition of oxygen and carbon in carbonates were performed at the Warsaw laboratory of ING PAN using a KIEL IV instrument attached on-line to the Delta Plus mass spectrometer in the dual inlet system. The sample preparation followed the classic McCrea technique. The sample mass was adjusted based on the XRD quantitative analysis to contain ~100 µg of a carbonate. The international NBS 19 standard was run after each ten-sample set. The results are reported with respect to the PDB standard. The measurement accuracy is 0.03‰ for  $\delta^{13}\text{C}$  and 0.07‰ for  $\delta^{18}\text{O}$ .

Selected samples in a natural state were carbon or chromium-coated and observed under SEM equipped with EDS detector in order to verify XRD mineral identification and to obtain information on crystal size, morphology and arrangement. Ten <0.2 µm fractions from the Woźniki profile were K-Ar dated at the Krakow laboratory of ING PAN, following the methodology of Środoń *et al.* (2006).

Apatite separation and fission track analysis followed the procedure by Anczkiewicz *et al.* (2013). The apatite fission track (AFT) dating method is a well established technique used to unravel thermal history experienced by rocks both during burial and during their movement towards the surface (Wagner & Van den Haute, 1992; Donelick *et al.*, 2005). Fission tracks are totally

annealed at temperatures higher than about 120°C, but partial resetting occurs above 60°C. Some variations in the annealing kinetics result from differences in the chemical composition of apatites (e.g. Barbarand *et al.*, 2003).

10–30 apatite crystals clean and free of defects and inclusions were selected for analyses. Data were analysed and ages calculated using the Zeta value for CN5  $\zeta_{\text{CN5}}$  of 348.19±6.5 and the Trackkey 4.2 program (Dunkl, 2002).

All quoted AFT ages are “central ages” (weighted mean ages  $\pm 1\sigma$ ) of Galbraith & Laslett (1993), and the variation of single grain ages was assessed using the % age dispersion of the central age and the chi-square test (Galbraith, 1981; Green, 1981). The fission track ages and the length data were modelled using a multi-kinetic model (Ketcham *et al.*, 2007) employing the HeFty software (Ketcham, 2005). This is a numerical search routine based on a data-driven approach using Monte Carlo methods. The result defines time-temperature “envelopes” that contain all randomly generated acceptable paths that pass baseline statistical criteria and conform to a set of user-defined geological criteria. For a comprehensive overview of fission-track methods and their modelling techniques, the reader is referred to Donelick *et al.* (2005), Ketcham (2005) and Braun *et al.* (2008).

## RESULTS

### *Mineral identification*

The mineralogical data are presented in Table 1. The mineral composition of the investigated profiles is rather monotonous (Fig. 2a). Major components are quartz, dioctahedral 2:1 minerals, kaolinite, calcite, and dolomite or Ca-dolomite. Common minor components are K-feldspar, albite, chlorite, hematite, goethite, pyrite and anatase. Occasionally traces of siderite were identified. In two Lipie samples marcasite was identified along with pyrite close to a coal layer (Fig. 2a). In and below the bone bed in Krasiejów abundant palygorskite is present (Fig. 2b), in agreement with earlier reports (Bzowska & Racka, 2006). Two samples at the bottom of the Schilfsandstein series in Woźniki contain gypsum, jarosite and abundant apatite, probably fluorapatite (300 reflection at 2.70 Å). The soil horizon among the Ladinian dolomites in Woźniki most probably

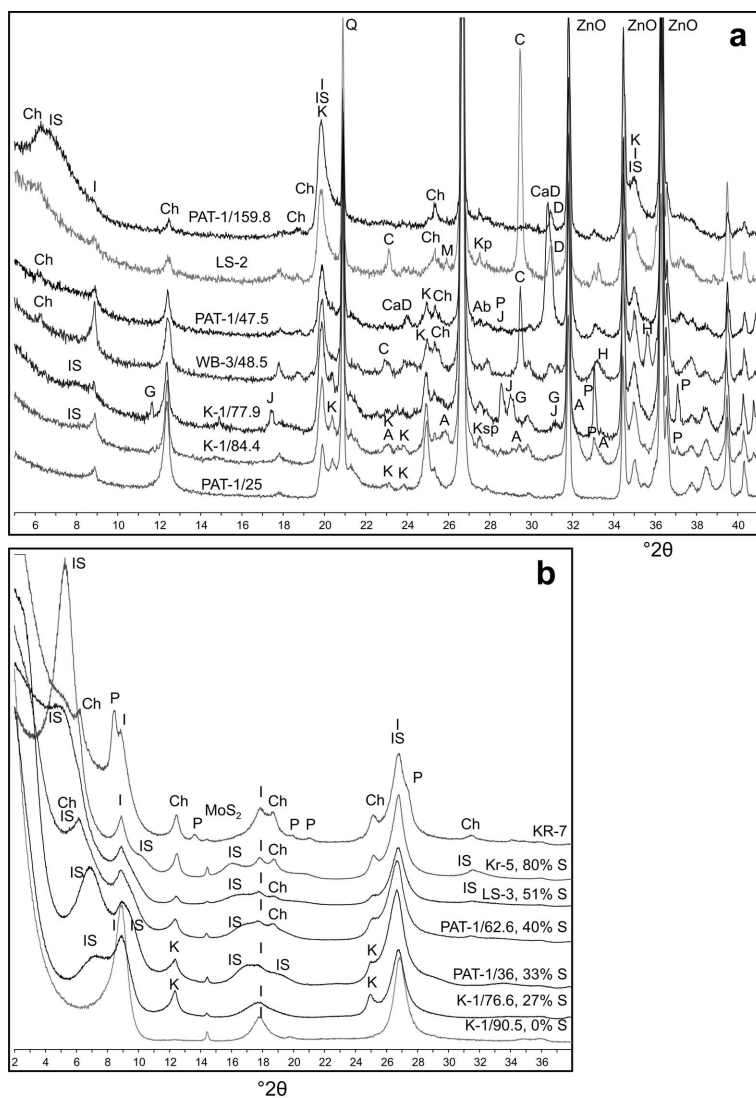


FIG. 2. XRD patterns of (a) bulk rock random preparations with ZnO as internal standard, illustrating mineral composition of the Keuper fine clastics, from illite-smectite to kaolinite-dominated clay fraction, (b) oriented glycolated preparations from  $<0.2 \mu\text{m}$  fractions with  $\text{MoS}_2$  as internal standard, illustrating the palygorskite admixture and the variation of illite-smectite composition. IS – illite-smectite, I – illite, Ch – chlorite, K – kaolinite, Ab – albite, Ksp – potassium feldspar, G – gypsum, C – calcite, D – dolomite, CaD – Ca-dolomite, P – pyrite, M – marcasite, H – hematite, J – jarosite, A – apatite.

contains dawsonite ( $\text{NaAlCO}_3(\text{OH})_2$ ), as indicated by a weak XRD peak at  $5.69 \text{ \AA}$ , though not confirmed under SEM. Dawsonite is a rare mineral of alkaline environments, often accompanying dolomite (Worden, 2006, and references therein).

The dioctahedral 2:1 mineral group consists of  $2M_1$  illite/mica and illite-smectite of 1Md to

turbostratic tri-dimensional structure. Only in three samples pure illite without illite-smectite was detected (Fig. 2b). A  $d_{001} = 9.94\text{--}9.96 \text{ \AA}$ , based on 002 and 005 reflections, not displaced after glycolation, indicates pure K-illite, without detectable  $\text{NH}_4$  substitution. Illite-smectite minerals range from R0 80%S (percent smectite layers) to R1

24%S (Fig. 2b), according to the identification based on peak position techniques (Środoń *et al.*, 2013), applying the calibration by peak positions of pure bentonitic illite-smectites (Środoń *et al.*, 2009). 060 reflection of the 2:1 clay group, indicative of an Fe content in the structure ranges from 1.501 Å (Al-rich composition) to 1.506 Å (0.34 Fe/O<sub>10</sub>(OH)<sub>2</sub>; Heuser *et al.*, 2013). The textures of 2:1 minerals observed under SEM seem indicative of a dominant sedimentary origin, characterized by irregular flat particles of micrometric size, often covering tangentially rounded quartz grains (Fig. 3a). The textures indicating authigenic growth of clays are rare, being more abundant only in the Krasiejów clays (Fig. 3b).

Kaolinite can be characterized more precisely only if it is relatively abundant and in all such samples it appears well-ordered. Kaolinite identified by SEM occurs predominantly as small irregular flat particles, thicker than 2:1 clays, in the Rhaetian samples occasionally associated with euhedral quartz crystals (Fig. 3c). A few large flat particles, resembling pseudomorphs after micas and more complete booklets (Fig. 3d) were also spotted. The presence of K<sub>2</sub>O in some of such particles may indicate remnants of primary mica or incipient authigenic illitization. Chlorite is a minor component almost always accompanied by dominant kaolinite (Table 1). In samples where it dominates kaolinite, chlorite is Mg-rich and non-expandable (Fig. 2b). Authigenic chlorite morphologies were not observed.

Sample Krasiejów 4 contains very delicate fibres filling locally the pore space (Fig. 3e) and growing on the surfaces of flat clay particles. Most probably the fibres represent palygorskite, but are too thin to confirm the identification by EDS. Rare incipient fibres were found also in the Krasiejów 5 sample (Fig. 3b), although XRD did not detect palygorskite.

Dolomite was identified by the most intense peak at 2.888–2.890 Å and Ca-dolomite by the peak in the 2.890–2.908 Å range (Table 1) and by EDS analyses in the SEM (distinction from ankerite due to lack of Fe). Most often dolomite and Ca-dolomite occur separately, but in the upper part of the Patoka profile the coexistence of the two minerals is common (Table 1). Dolomite often coexists with calcite, but typically either dolomite or calcite is definitely dominant (Table 1). Most of calcite and dolomite are finely dispersed; larger idiomorphic crystals are rare.

The XRD characteristics of hematite (very broad 104 peak at 2.702 and narrow 110 peak at 2.522 Å,

Fig. 2a) are indicative of an origin from a goethite precursor via a low-temperature topotactic dehydration reaction (Brindley & Brown, 1980, p. 372). These crystals are intimately dispersed in clay and so small that in most cases cannot be identified by SEM. The BSE technique combined with EDS detected uneven concentrations of iron in clay-hematite aggregates (Fig. 3f). Surfaces of such aggregates are covered by clay particles, but accumulations of elongated hematite particles with dimensions of 150–30 nm can be observed if the aggregates are broken (Fig. 3g). Gypsum was identified in two samples at the bottom of the Schilfsandstein in Woźniki in the form of large idiomorphic crystals occurring locally, accompanied by abundant pyrite and native sulfur (Fig. 3h).

#### *Quantitative mineral relationships*

Very clear quantitative correlations exist among clay minerals and quartz (Fig. 4, Table 1). Kaolinite and illite 2M<sub>1</sub> are correlated positively with quartz, while illite-smectite correlate negatively. Also the *d*<sub>060</sub> of 2:1 clay correlates negatively with quartz, indicating that larger values, i.e. more Fe-rich compositions, characterize the 1Md clay. These relations are best visible for the Patoka well, which displays a broad range of compositional variation, but can also be clearly observed in the Woźniki profile; thus they characterize the entire Keuper section. Carbonates are absent in the Rhaetian rocks and almost absent in the Schilfsandstein. Dolomite is enriched clearly below the Schilfsandstein and in the bottom part of Patoka, while calcite is enriched in the upper part of Woźniki and in the entire Kobylarz profile. The distribution of carbonates is highly bimodal: rocks rich in calcite are poor in dolomite and *vice versa*. In the Patoka and Kobylarz profiles, containing multiple alterations of soils and shales, a clear calcite and hematite enrichment of soil horizons, typical for calcisols, is observed (Table 1). Pyrite occurs essentially in green and grey, hematite-free rocks, but otherwise no regularities were observed, except for a clear pyrite enrichment at the onset of kaolinite-rich sedimentation (Schilfsandstein (Carnian) in Woźniki and the top of Norian in Patoka). The concentrations of potassium feldspar and chlorite show regional variations: feldspar is more abundant in the east, while chlorite is abundant in the west (Table 1). Also %S varies regionally; only R1 clays of <35%S were detected in the eastern profiles,

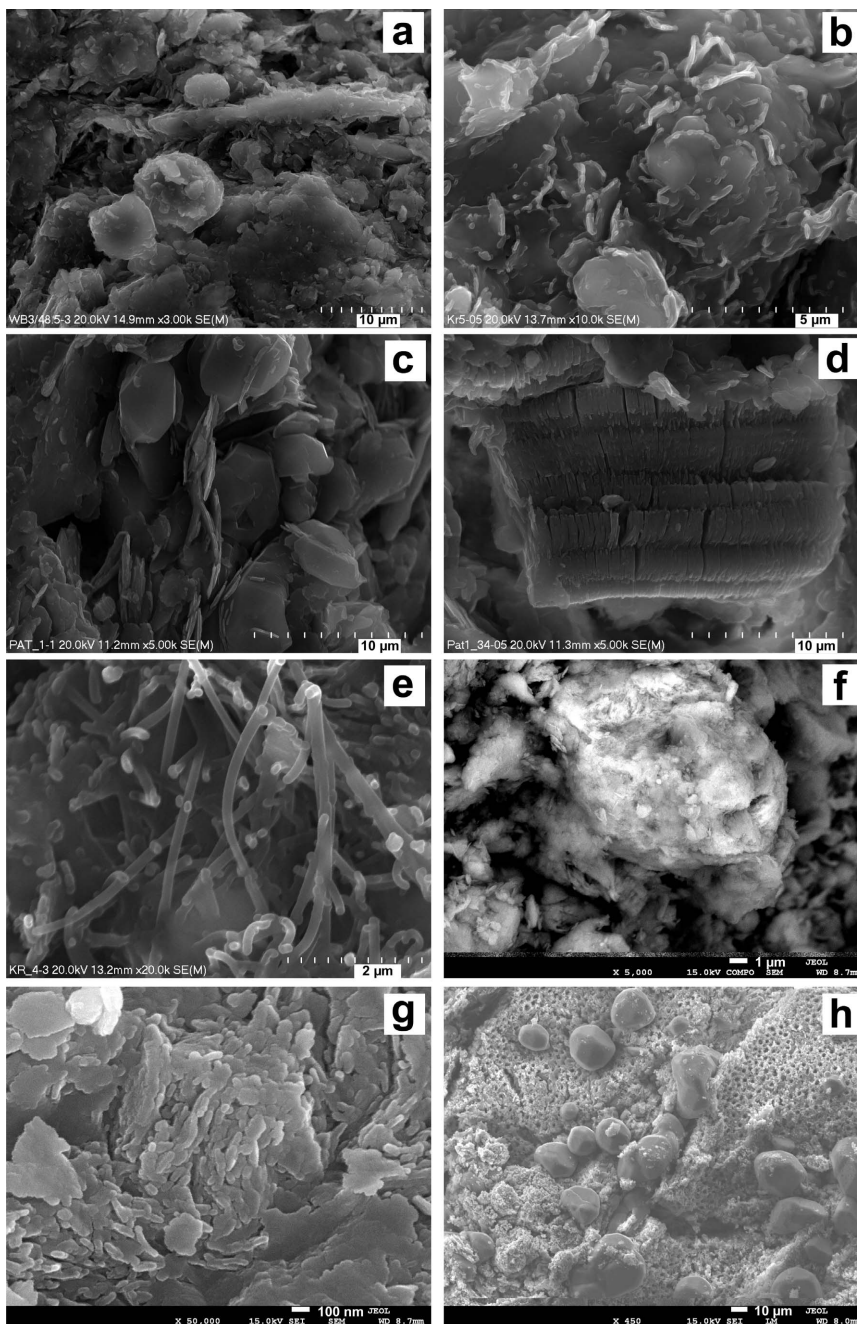


FIG. 3. SEM photographs documenting morphology of the identified minerals. (a) Detrital morphology of illite particles tangentially covering rounded quartz grains; (b) possible incipient growth of palygorskite from surfaces of detrital particles; (c) dispersed crystals of kaolinite and authigenic quartz; (d) slightly rounded kaolinite "booklet"; (e) fibres of palygorskite filling pore space; (f) clay-hematite aggregate covered tangentially by clay particles, broken in the upper part (BSE image with accumulations of hematite in light colour); (g) accumulation of fine hematite crystals surrounded by bigger clay particles (high magnification of f); (h) native sulfur crystals on fine-grained pyrite substrate.

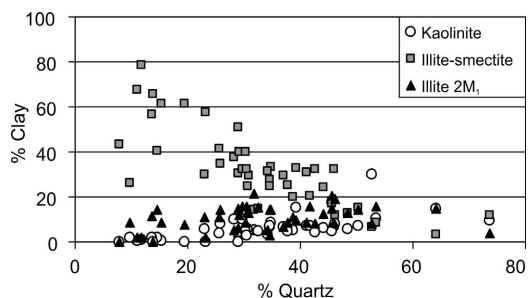


FIG. 4. Compositional trends of clay fraction with respect to quartz content, used as a proxy for the grain size. Data for the Patoka profile.

while in the west both R1 clays and R0 up to 80%S are present.

In the Patoka well the mineralogical composition evolves systematically with depth, from quartz- and kaolinite-rich rocks at the top to illite-smectite rich at the bottom (Fig. 5). To classify this variability, the profile was divided into four parts, A, B, C and D, and the corresponding mean values for clastics (i.e. excluding carbonate rocks) were calculated (Table 1). Clear changes of slope of this general trend occur at ~50 and 150 m; between these depths the mineralogical composition is relatively constant. %S follows this trend, from R1 at the top to R0 at the bottom, i.e. opposite to the burial diagenetic trends. Chlorite in Patoka is most abundant in the middle part of the profile.

The Patoka profile was regarded in this description as reference, because of its largest mineralogical variability, and the remaining occurrences were compared to Patoka. The Krasiejów and Lipie sites are closer geographically and resemble compositionally the bottom of the Patoka profile (parts C and D): they are low in quartz and kaolinite and high in

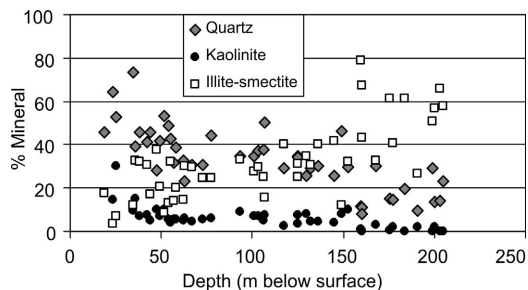


FIG. 5. Major mineral trends with depth in the Patoka profile.

carbonates and 2:1 minerals. Also the expandability of illite-smectite is similarly high.

The Woźniki profile starts from the Ladinian dolomites, which are overlain by three distinct parts, based on mudstone mineral composition. The lowest part resembles Patoka D, because of low quartz and kaolinite contents and high carbonate and 2:1 mineral contents. A characteristic unique feature is the presence of samples with pure illite, without mixed-layer illite-smectite. The middle part (Schilfsandstein) resembles Patoka B, but is enriched in kaolinite. The upper part has a similar composition to Patoka C.

The Kobylarz profile is very homogenous and closely resembles Patoka C. The Koziegłowy profile is much more heterogenous. On average it also resembles Patoka C, but the two samples, representing the part identified as Schilfsandstein, resemble the Schilfsandstein composition in Woźniki, and also the Patoka B section. Similar to the Woźniki profile, pure illite without illite-smectite was found below Schilfsandstein.

#### Distribution of geochemical data

Sodium, B, Sr, Cl and Ba increase systematically with depth in the Patoka profile (Table 2 (deposited), Fig. 6). The  $\text{Na}_2\text{O}$ , B and Sr curves (Fig. 6) are analogous to the mineral curves (Fig. 5), displaying changes of slope at ~50 and 150 m. Interestingly, the Sr content is not related to the carbonate content, which varies significantly in the Patoka profile. Also the  $\text{Na}_2\text{O}$  content is not related to the albite, which occurs in constant trace amounts. In the Ba profile only a rapid increase at 150 m is apparent. Mo also increases down the profile, but the maximum values are reached at 125–152 m depth, decreasing thereafter. Only Zr shows a clear opposite trend, explained by positive correlation with quartz (Fig. 7), which implies that biogenic silica is not present in measurable quantities. Local concentrations of one order of magnitude are observed for Pb in the upper part of the profile and for U and V in the lower part. Carbon measured chemically is essentially inorganic, as is indicated by the good correlation between C measured and C calculated from the calcite and dolomite contents (Fig. 8). The Rhaetian part of the profile (A) is exceptionally enriched in Al, Si and Ti, but is poor in Fe, Mn, Mg, Ca, K and P.

By analogy with the mineral data, the levels of  $\text{Na}_2\text{O}$ , Sr and Ba render the Krasiejów and Lipie

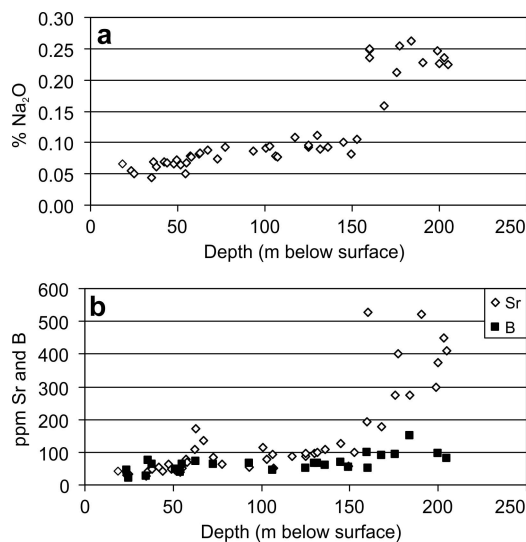


FIG. 6. The most apparent chemical trends with depth in the Patoka profile.

sites similar to the bottom part (D) of the Patoka profile. The Mo levels are also similar (Krasiejów) or even much higher (Lipie). A positive Pb anomaly was recorded in Lipie. The Zr/quartz ratios are clearly elevated in Lipie. The bone bed in Krasiejów (Kr-4) does not differ chemically from other samples, even in P<sub>2</sub>O<sub>5</sub>.

The Na<sub>2</sub>O, Sr, and Ba contents in the Woźniki, Koziegłowy, and Kobylarz profiles are similar to Patoka C, with a few major positive anomalies in Sr, Ba and Mo concentrations. Cl and B concentrations have been measured for Koziegłowy and are at Patoka C/D levels. The Zr/quartz ratios in the three profiles are similar to Patoka (Fig. 7). In all three profiles, positive Cu anomalies were recorded (Table 2). At the bottom of the Schilfsandstein in the Woźniki profile, the

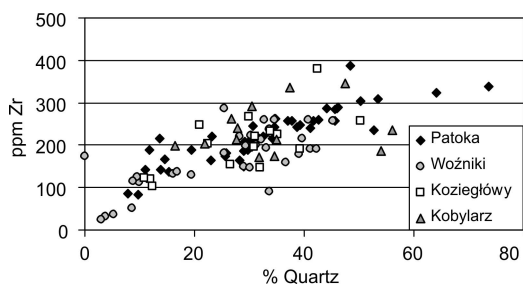


FIG. 7. Strong positive correlation of ppm Zr and quartz content.

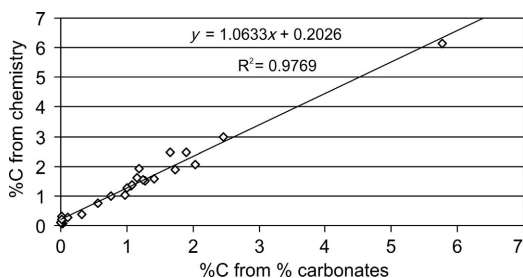


FIG. 8. Verification of the quantitative XRD data using total carbon chemical analysis. Data for the Patoka profile.

sample with apatite contains almost 5% P<sub>2</sub>O<sub>5</sub> (almost 70× enrichment over other mudstones) and represents a major geochemical anomaly – increased Ba, Co, Cu, Mo, Ni, Pb, Sc, Th, U, Y and REE, including a radically increased Sm/Nd ratio (0.26) and decreased La/Ce ratio (also 0.26). Except for P, the most enriched elements are Y (23×) and the REE. The pattern of REE enrichment is typical for apatites and controlled by crystallochemistry (Pan & Fleet, 2002) – lowest for LREE and HREE (6–8×) and highest for Sm, Eu, and Gd (>30×). A sample taken few metres above the apatite-bearing profile has increased Co, Cu, Mo, Ni and U contents. The Schilfsandstein sections of Woźniki and Koziegłowy resemble the composition of major elements the Rhaetian part of Patoka – elevated Si, Al and Ti contents and low Mn, Mg and Ca contents. However Fe, K and P are not depleted like in the Rhaetian horizons.

Water loss measured at 200°C equals ~1.5 times the water loss at 100°C, which is typical for Ca-smectites (Środoń & McCarty, 2008). This water loss is strongly correlated with the amount of 2:1 minerals (Fig. 9). The relationship is not linear, as the more clay-rich samples are more smectitic.

The isotopic composition of carbon and oxygen in carbonates was measured for a set of samples, selected due to the presence of one dominant carbonate phase (calcite, dolomite or Ca-dolomite), according to the quantitative XRD analysis, which represented the entire section. The δ<sup>18</sup>O values range from +1.90 to –6.78, and δ<sup>13</sup>C from +0.18 to –9.70 (Table 2). Two controls over the isotopic composition can be detected – mineralogy and the position in the profile, which was established using geochemical indicators (see below). If only calcite data are analysed, they form a clear trend towards lighter isotopic C and O composition in the younger

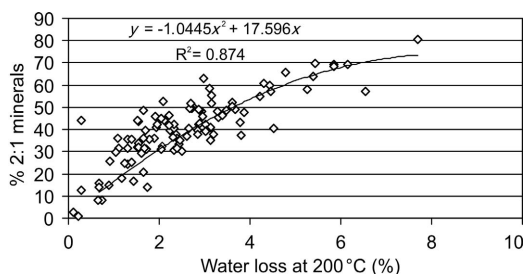


FIG. 9. Non-linear positive correlation of water loss and the content of 2:1 minerals, reflecting the variation in the degree of illitization.

rocks (from the horizon IV towards I: Fig. 10). Dolomites do not differ detectably from Ca-dolomites and both have oxygen isotopes clearly heavier than calcites, while their carbon isotopes are either heavier or comparable to the calcites.

The content of total organic carbon is available for the Patoka and Koziegłowy profiles (Table 2); single measurements from Woźniki, Patoka, and Lipie clay-pits are also available (Marynowski & Wyszomirski, 2008). The values are generally low, <0.5%. Higher values, reaching >2%, were found in the Schilfsandstein samples in both profiles and in Lipie, where coals (jets) were also found. Interestingly, the upper part of Patoka profile (B), which is mineralogically similar to the Schilfsandstein, does not have high TOC contents.

#### K-Ar data

Ten K-Ar dates were obtained for <0.2  $\mu\text{m}$  fractions from the Woźniki profile (Table 3). Four of them are older than the stratigraphic age and six

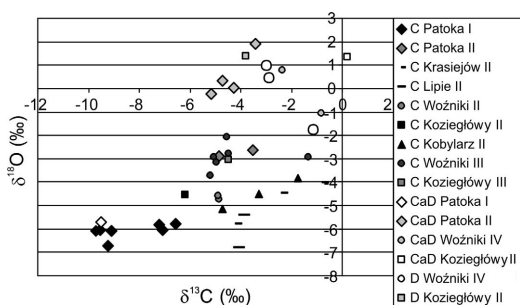


FIG. 10. Stable isotope composition of calcite, dolomite and Ca-dolomite from all the investigated locations. Empty or light symbols for dolomite and Ca-dolomite, black or dark symbols for calcite. Different symbols used for profiles and their chemostratigraphic zones to illustrate also regional and temporal variations.

are younger. The two groups contain a range of samples, from almost pure illite to dominant illite-smectite of similar expandability plus variable amounts of kaolinite. Samples with higher  $\text{K}_2\text{O}$  contain less kaolinite and have lower IS/I ratio.

#### AFT data

Results of AFT analyses are presented in Table 4 and Fig. 11. The analysed samples were shown to be fluoroapatites, based on a small etch-pit size (Dpar in Table 4), similar to the Durango fluoroapatites (Barbarand *et al.*, 2003; Donelick *et al.*, 2005). Central ages of these samples range from  $166.2 \pm 9.0$  to  $120.7 \pm 8.0$  Ma, which are much lower than the stratigraphic ages. Only one sample gave an age of  $206.1 \pm 38.1$  Ma, close to the Triassic stratigraphic age (PAT-1/51.5-7).

TABLE 3. K-Ar data for <0.2  $\mu\text{m}$  fractions of Woźniki samples.

Sample	% $\text{K}_2\text{O}$	% $^{40}\text{Ar}^*$	$^{40}\text{Ar}^*$ (pmol/g)	Age (Ma)	Error (Ma)
K-1/23.8	5.47	78.93	1818.7	<b>217</b>	2
K-1/41.4	5.74	89.54	2380.1	<b>267</b>	1
K-1/44.7	5.01	76.98	1238.6	<b>164</b>	1
K-1/57.5	5.96	77.09	1572.3	<b>175</b>	1
K-1/73.6	5.26	70.94	1411.6	<b>177</b>	2
K-1/76.6	5.28	80.26	1800.5	<b>223</b>	1
K-1/85.4	6.2	80.81	2015.4	<b>213</b>	1
K-1/90.5	6.48	73.81	1952.3	<b>198</b>	1
K-1/94.7	6.46	87.24	2499.2	<b>251</b>	1
K-1/96	6.26	74.38	1938.3	<b>203</b>	1

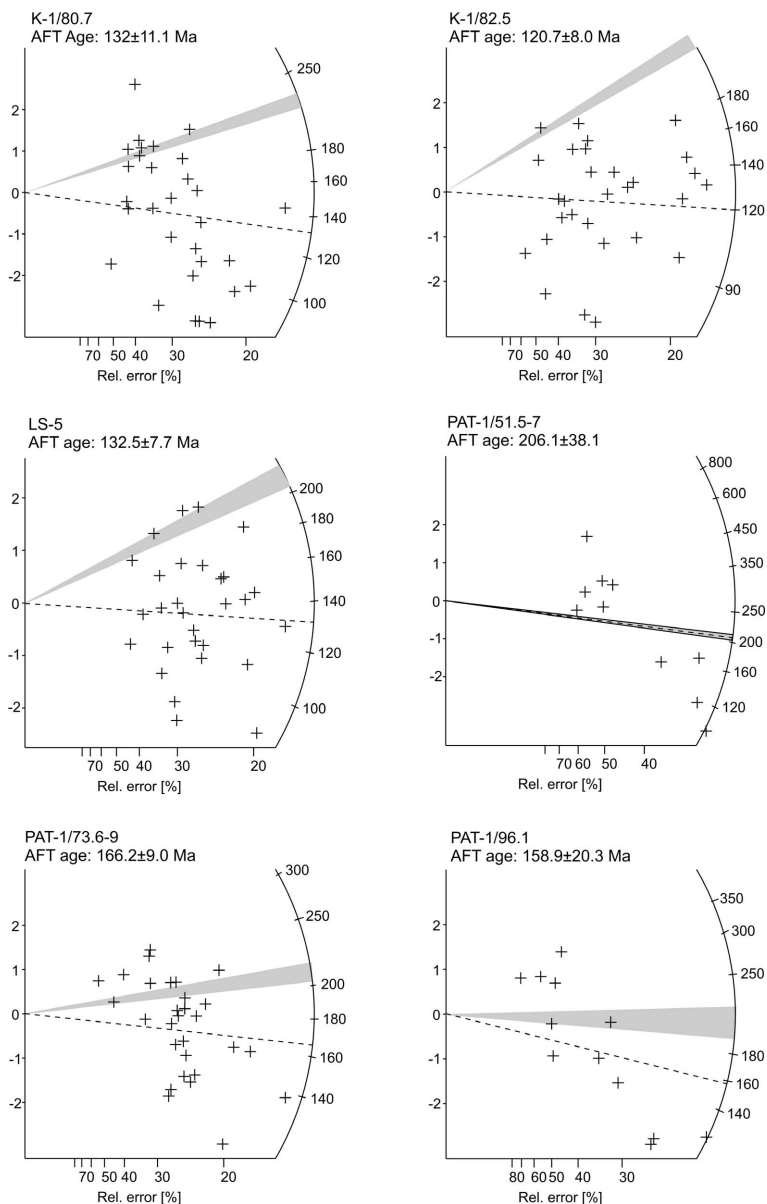


FIG. 11. Radial plots of fission track ages. Central age is defined by the dashed line, stratigraphic age is represented by the shaded area.  $x$  scale represents the precision of individual grain age estimate ( $1/\sigma$ ), calibrated as percent relative standard error, whilst  $y$  scale, calibrated in units of standard error ( $\sigma$ ), represents dispersion of ages from the mean value. The age of each crystal may be determined by extrapolating a line from the origin on the left through the crystal's  $x$ ;  $y$  coordinates to the radial age scale (Galbraith, 1990). Radial plots were drawn using the program TRACKKEY, version 4.2 (Dunkl, 2002).

Three samples yielded single populations of grain ages as shown by  $P(\chi^2)$  values (Table 4) greater than 5% (Galbraith, 1981; Green, 1981), and the

remaining three samples showed more than one population of apatite in the same sample ( $P(\chi^2) < 5\%$ ). Both the oldest and the youngest AFT ages

TABLE 4. AFT results. U – the concentration of uranium evaluated by the Trackkey 4.2 software (Dunkl, 2002); pd – density of induced tracks in external detector which cover dosimeter (glass CN5)( $\times 10^6$  tracks for  $\text{cm}^{-2}$ ), Nd – numbers of counted tracks; ps – density of spontaneous tracks ( $\times 10^6$  tracks for  $\text{cm}^{-2}$ ), Ns – numbers of counted spontaneous tracks; pi – density of induced tracks in external detector (mica) ( $\times 10^6$  tracks for  $\text{cm}^{-2}$ ), Ni numbers counted induced tracks. P ( $\chi^2$ ) given in % is the probability of homogeneity of the apatite population, i.e. a measure of the dispersion of ages of analysed apatite crystals (Galbraith, 1981; Green, 1981). Age is the central age of a sample (Galbraith & Laslett, 1993), counted by using calibration method zeta (Hurford, 1990) and the dosimeter (glass) CN5. Length $\pm$ SE is an average length of confined tracks plus standard error, SD – standard deviation of the length. Dpar is the mean fission-track etch pit diameter parallel to the crystallographic *c* axis of apatite grain. At least four Dpar measurements per apatite grain, analysed for AFT age and/or confined track length, have been made.

Sample no.	Rock type	Stratigraphy	No. of crystals	U (ppm)	Dosimeter pd	Nd	Spontaneous ps	Ns	Induced pi	Ni	P ( $\chi^2$ ) (%)	Age (Ma) $\pm 1\sigma$	Length $\pm$ SE ( $\mu\text{m}$ )	SD	Number of tracks	Dpar ( $\mu\text{m}$ )
K-1/80.7	Sandstone	Karnian: 228–217 Ma	30	19.9	1.171	3699	1.189	637	1.945	1042	0	132.2 $\pm$ 11.1	12.90 $\pm$ 0.12	1.28	111	1.88
K-1/82.5	Sandstone	Karnian: 228–217 Ma	30	16.7	1.184	3699	0.908	655	1.527	1102	3.5	120.7 $\pm$ 8.0	12.91 $\pm$ 0.15	1.54	106	1.91
LS-5	Sandstone	Norian: 217–204 Ma	30	21.5	1.15	3587	1.16	752	1.742	1129	17.7	132.5 $\pm$ 7.7	13.30 $\pm$ 0.12	1.22	105	2.17
PAT-1/51.5	Sandstone	Norian: 217–204 Ma	10	9.7	1.135	3564	0.867	125	0.922	133	2.1	206.1 $\pm$ 38.1	14.43 $\pm$ 0.26	1.19	20	2.3
PAT-1/73.6	Sandstone	Norian: 217–204 Ma	30	19.4	1.203	3806	1.445	896	1.811	1123	29.9	166.2 $\pm$ 9.0	13.24 $\pm$ 0.14	1.47	107	2.34
PAT-1/96.1	Sandstone	Norian: 217–204 Ma	12	12.3	1.108	3564	0.882	196	1.147	255	6.82	158.9 $\pm$ 20.3	13.62 $\pm$ 0.36	1.74	23	2.19

belong to the latter category. The measured mean track lengths (MTL) are significantly reduced and vary from 14.43  $\mu\text{m}$  to 12.90  $\mu\text{m}$ . The samples have rather unimodal track length distributions. The MTL are very well correlated with the AFT ages, including the oldest sample.

## INTERPRETATION

### *High-temperature overprint*

K-Ar dates younger than the stratigraphic age in some samples and older than the stratigraphic age in others (Table 3) indicate that the 2:1 clay minerals in the Keuper rocks contain a mixture of detrital and authigenic illitic material, i.e. that the rocks underwent *in situ* illitization long after the deposition. This process produced both illite-smectite and discrete illite, as the youngest dates are not correlated with the high ratio of illite-smectite to discrete illite. The vertical distribution of %S in the Patoka profile, opposite to the normal diagenetic trend, indicates that the illitization is not a product of burial diagenesis. This conclusion is consistent with the available information on the post-Triassic burial history of the area, where only a few hundred metres of the Jurassic and Cretaceous sediments can be accounted for (Marek & Pajchlowa, 1997; Botor *et al.*, 2012).

On the other hand, the area has been affected by a widespread Mesozoic hydrothermal event, documented by the Pb-Zn ore deposits in Triassic rocks (Heijlen *et al.*, 2003) and K-Ar dates of illite-smectite from the Carboniferous bentonites (Środoń *et al.*, 2006). Such an event of Late Jurassic or even younger age explains all K-Ar data collected in this study (Table 3). It is a feasible assumption that the coarse-grained rocks were more accessible for these hot fluids and as a result their illitization is more advanced, offering the upper estimate of the temperature of penetrating fluids,  $\sim 125^\circ\text{C}$  (Table 1), consistent with 80–158°C temperature range of Pb-Zn deposit formation, based of the fluid inclusions in sphalerite (Kozłowski & Górecka, 1993; Kozłowski, 1995). The hydrothermal activity in the area, though of lower temperature, had already started locally in the Norian, as documented by the hydrothermal component detected in the Woźniki limestones, overlying directly the Steinmergel sediments in many places (Szulc *et al.*, 2006).

Among the 44 samples investigated in the  $<0.2 \mu\text{m}$  fraction, the three samples from the

Lower Gipskeuper in Woźniki and Kozieglówy are exceptional, containing essentially pure illite, instead of an illite plus illite-smectite mixture, and being almost free of kaolinite (Table 1, Fig. 2b). Their K-Ar ages (Table 3) indicate that they are mixtures of detrital and authigenic illite, so most probably they also are products of the Mesozoic hydrothermal event which caused illitization of both smectite and kaolinite. Both K-Ar ages and the average value of  $d_{060}$  (Table 1) indicate that these are not lacustrine Fe-illites, known from the European Keuper in other locations (Jeans *et al.*, 1994). A possible explanation of such local, elevated levels of illitization is a tectonic-related conduit for hot fluids, opened at the contact of very competent massive dolomite rocks with the overlying clastics.

The AFT dates support the reconstruction of thermal history based on illite. All but one sample gave AFT ages significantly younger than the stratigraphic ones, suggesting at least partial thermal resetting (post-depositional temperatures above  $60^\circ\text{C}$ ). The  $P(\chi^2)$  values far from 100 indicate that the resetting was not complete, which implies maximum temperatures not higher than 100–120°C (Anczkiewicz *et al.*, 2013). Older ages are correlated with longer tracks, which indicate shorter residence of these samples in the apatite partial annealing zone (APAZ).

The track length distributions were modelled assuming an Upper Carboniferous or Ladinian detrital age of apatites, according to the expected sediment sources in the Moesian microplate (Fig. 1). Modelling (Fig. 12) yielded results very insensitive to the detrital age, indicating that post-depositional reset was almost complete, and thus the maximum palaeotemperatures were close to  $120^\circ\text{C}$ . The ages of these palaeotemperatures were evaluated as 160–170 Ma in Woźniki, in perfect agreement with the youngest K-Ar date from this profile, 160–170 Ma in Lipie, and 190–200 Ma in Patoka. According to these models the samples left APAZ at  $\sim 100$ –120 Ma.

For the Lipie and Woźniki profiles, where unoxidized organic matter was found, the maximum palaeotemperature estimates from illite-smectite ( $90^\circ\text{C}$  and  $120^\circ\text{C}$ , respectively – Table 1) and from AFT modelling ( $110^\circ\text{C}$  – Fig. 12) can be compared with organic maturity indicators. For the green shales from Lipie, the predominance of less stable  $\text{C}_{31}\text{R}$  over  $\text{C}_{31}\text{S}$  homohopane and the detection of unsaturated pentacyclic triterpanes

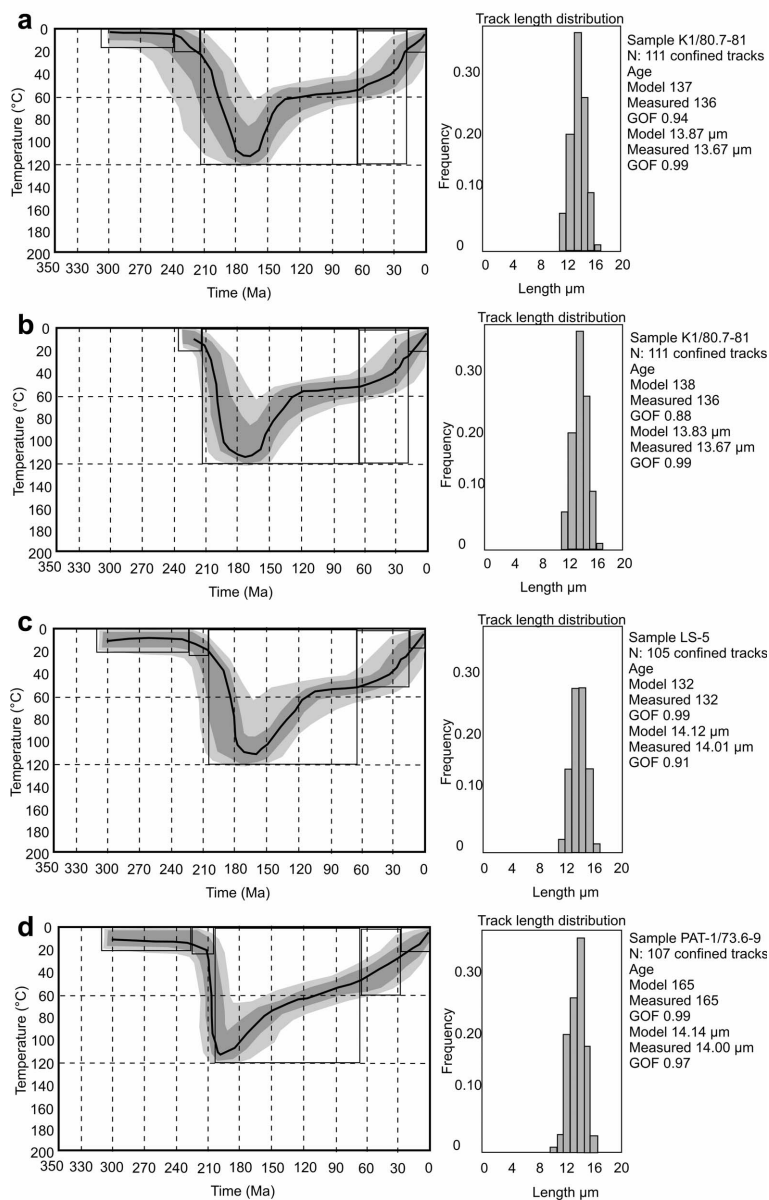


FIG. 12. AFT time-temperature paths obtained from inverse modelling by the HEFTY program, using the Monte Carlo algorithm (Ketcham, 2005). Predicted apatite fission-track data were calculated according to the Ketcham *et al.* (2007) annealing model and  $D_{\text{pars}}$  were used as the kinetic parameter. Shaded areas mark envelopes of goodness-of-fit (GOF)  $\pm 0.5$ , and the thick lines correspond to the thermal history with the best fit (= maximum GOF). Thermal paths outside the partial annealing zone are largely inferential as the fission-track data provide reliable information only in the temperature range 60–120°C (the exact temperatures depending on resistance to annealing and cooling rate). GOF gives an indication of the fit between observed and predicted data (values close to 1 are best). Mean track lengths are reported after  $c$ -axis projection and therefore differ from those listed in Table 4. The time-temperature boxes used as constraints apply the Upper Carboniferous or Ladinian detrital ages of apatites and the mean surface temperature for periods prior to the stratigraphic age and the Cenozoic. In between, a wide range of temperature between 120 and 10°C was used.

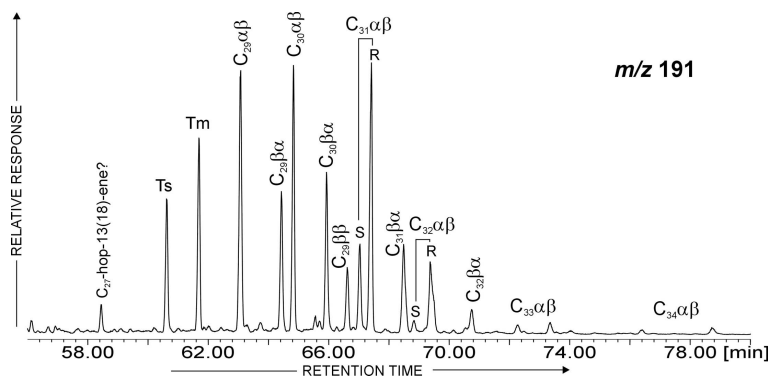


FIG. 13. Partial  $m/z$  191 mass chromatogram of a green clay enriched in terrestrial plant debris showing immature character of hopanes distribution. Woźniki well, 77.7m sample. DB-35 column was used.

(norneohop-13(18)-ene and neohop-13(18)-ene) and  $C_{30}$  as well as  $C_{31}$  hopanes with biological  $\beta\beta$  configuration (Marynowski & Wyszomirski, 2008) indicate very low OM maturation, equivalent of vitrinite reflectance  $R_o = 0.35\%$  (Peters *et al.*, 2005). A similar hopanes distribution, with lower concentration of unsaturated hopanes, but still revealing immature character (equivalent of  $R_o = 0.40\%$ ), was found in the Woźniki well samples, between 76.7 and 78.1 m (Fig. 13).

The organic indicators confirm more advanced alteration in Woźniki and generally low level of diagenesis, below oil window. Organic parameters are controlled by kinetics, so the evaluation of the maximum palaeotemperatures is not straightforward (e.g. Sweeney & Burnham, 1990). According to the measurements in oil wells from young sedimentary basins,  $R_o = 0.5\%$  corresponds roughly to 90–110°C (Suggate, 1998; Środoń *et al.*, 2006); thus the data for Lipie and Woźniki indicate palaeotemperatures below this range. A similar discrepancy between the estimates from illite-smectite and from an organic maturity indicator (vitrinite reflectance) was noted in the Carboniferous rocks in NE part of the Upper Silesian Coal Basin, which were affected by the same thermal event (Środoń *et al.*, 2006). This discrepancy is waiting for a convincing explanation.

The crystallization of illite involves incorporation of potassium, other cations similar to potassium ( $NH_4^+$ ,  $Rb^+$ ,  $Cs^+$ ), and B, which substitute for Si in the tetrahedral sheet (e.g. Środoń, 2010). Theoretically, potassium may originate from within the rock by dissolution of the detrital components (micas, feldspars) or it may be imported from outside the rock. To answer this

question, the ratio of  $\%K_2O$  to the sum of minerals potentially involved in the illitization reaction (clays and feldspars) was calculated and plotted vs. the degree of illitization expressed as  $\%S$  (Fig. 14a). The result is a clear indication of an open system showing the import of potassium into the rock during the illitization process, which is consistent with an open hydrothermal system.

Ammonium increases slightly along with  $\%K_2O$ , but the concentrations are close to the detection limit (Table 2), much lower than commonly encountered during burial diagenesis of sedimentary basins (e.g.

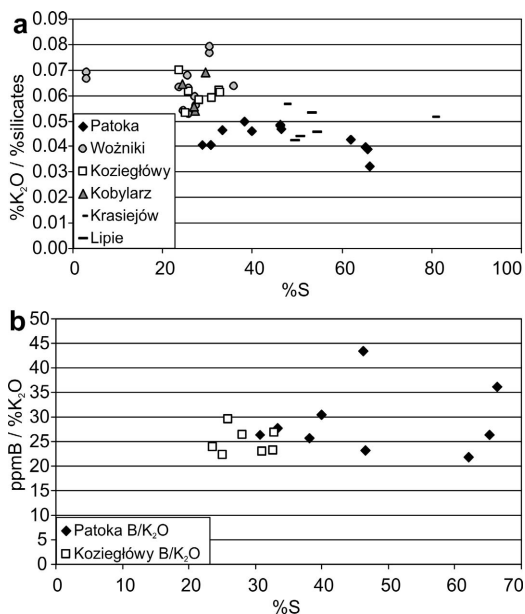


FIG. 14. Chemical changes of the bulk rock during diagenesis:  $K_2O$  (a) and B (b).

Środoń & Paszkowski, 2011). Apparently during illitization of these oxidized sediments the source of  $\text{NH}_4^+$  (OM undergoing parallel diagenesis: e.g. Środoń, 2010; Williams *et al.*, 2013) was very poor, as indicated by the low organic carbon content of these rocks (TOC: Table 2). Boron is quite abundant (20–150 ppm) and increases linearly with %  $\text{K}_2\text{O}$ , but the B/K ratio remains constant during illitization (Fig. 14b), similar to other studies (Środoń, 2010). Such decoupling of  $\text{NH}_4^+$  and B behaviour indicates a different source for B than the organic matter (cf. Środoń & Paszkowski, 2011).

Both Rb and Cs increase with  $\text{K}_2\text{O}$  but the trends are different. The correlation Rb- $\text{K}_2\text{O}$  is strictly linear, indicating a stable K/Rb ratio of ~200, which is typical for sedimentary rocks, indicating control by most common K-bearing minerals, i.e. K-feldspar and dioctahedral mica (Shaw, 1968). The correlation Cs- $\text{K}_2\text{O}$  is not linear. When the Cs/ $\text{K}_2\text{O}$  ratio is plotted against %S clear diagenetic enrichment in Cs with respect to K appears. It is an indication of an open system and of a selective incorporation of Cs by illite.

It seems feasible that the authigenic quartz in the coarsest mudstones (Fig. 3g) and local concentrations of Pb, Cu, Ba, U, V and Mo (Table 2) are also related to the Mesozoic thermal event, which deposited large Zn and Pb deposits just E and SE of the investigated area (Heijlen *et al.*, 2003) These hot fluids interacted with and remobilized metals from the Carboniferous porphyry copper deposits (Chaffee *et al.*, 1994) located under the eastern part of the investigated area (Fig. 1) or perhaps they signal other deposits hidden farther to the west.

Based on this reconstruction of the high-temperature hydrothermal overprint, it can be assumed that the clay fractions of original Keuper sediments were impoverished with respect to their present composition in K and the associated elements, and were dominated by kaolinite, dioctahedral smectite, and illite.

#### *Sedimentary and low-temperature diagenetic overprint*

The elevated concentrations of Na, B, Sr, Cl and Ba at the bottom of Patoka and in other western localities indicate contact with saline waters. The sedimentary and diagenetic history of the area implies that such contact may have happened twice – during sedimentation and during the infiltration of hydrothermal fluids, which caused illitization, and

which are well documented as being saline from the fluid inclusions in sphalerite (Kozłowski, 1995). The elevated contents of Na, B, Sr, Cl and Ba are characteristic of the most fine-grained sediments (compare Figs 5 and 6), which were least illitized because of the restricted penetration of fluids in low-permeability rocks. Such distribution may indicate that these elevated values signal saline conditions during sedimentation. In more porous sediments the original sedimentary waters were exchanged by the hydrothermal waters, and those in turn by meteoric waters. Analogous selective sedimentary pore water preservation in mudstones was documented for the Carpathian foredeep Miocene sediments (Środoń & Kawiak, 2011).

Low-temperature authigenic minerals include calcite, dolomite, Ca-dolomite, palygorskite, gypsum, jarosite, pyrite, marcasite, native sulfur, apatite and possibly dawsonite. Calcite and dolomite are considered sedimentary in origin and facies-bound because of their fine grain and the oxygen isotope composition controlled by stratigraphy (cf. Reinhard & Ricken, 2000). The largest distance between sample locations is less than 80 km; thus the observed isotopic variation most probably reflects the interplay between the supply of isotopically light meteoric waters and evaporation. The trend towards lighter isotopic composition of calcite at the top in Patoka, Woźniki, and Koziegłowy implies diminishing saline water influence, consistent with the progradation of the peripheral alluvial fan zone, recorded also by the coarser grain composition of the Patoka mudstones. The change of climate towards more humidity would produce the same effect. Calcites from the same age zone (II) are isotopically heavier in Patoka than in other profiles; this is consistent with the location of Patoka farther into the basin centre, compared to other profiles (Fig. 1).

Dolomites fit this picture possibly as markers of the episodes with higher evaporation – in a given sedimentary setting the oxygen in dolomites is always isotopically heavier than in calcites. All dolomite samples except one from the top zone (I) in Patoka, where the fresh water influence is strongest, are isotopically heavier than the Upper Triassic Thetyan seawater (–1 per mil  $\delta^{18}\text{O}$ : Veizer *et al.*, 1997), thus periodic marine incursions cannot be excluded. Such periodic incursions are further supported by the fact that increased evaporation alone seems to produce calcite, as evidenced by the increased calcite content of the soil horizons.

Palygorskite is present only in one thin layer in Krasiejów in association with calcite but not dolomite. The oxygen in calcite associated with palygorskite is significantly heavier than the overlying mudstone without palygorskite (Table 2), although far below the marine water level. This indicates fresh water, concentrated by evaporation, as the environment of palygorskite crystallization. The carbon in calcite associated with palygorskite is the heaviest among the analysed samples, which may be the clue to the specific conditions of palygorskite crystallization. Several explanations are possible (e.g. organic productivity, temperature: cf. Reinhard & Ricken, 2000); thus the problem cannot be solved without palygorskite-calcite isotopic analysis, which should provide the temperature of crystallization. In any case, the occurrence of palygorskite in thin horizons, characteristic also for other areas of the European Keuper (Jeans, 2006), is indicative of an episodic change of the sedimentary environment, and the lack of palygorskite in the rocks of corresponding age in other profiles implies that this change is local.

Gypsum is an obvious indicator of the evaporitic environment, recorded in the most saline part of the profile (abundant dolomite: Table 1). Most probably it was originally much more abundant, but was dissolved during later geological history and in particular during the penetration of hydrothermal waters. The pseudomorphs of gypsum and halite crystals are commonly observed in the Silesian Keuper rocks (Szulc *et al.*, 2006).

Pyrite and marcasite most probably formed at the expense of detrital hematite, deposited in a reducing environment. Marcasite is clearly associated with the coal matter while native sulfur indicates extreme reducing conditions. Apatite concentration at the bottom of the Schilfsandstein in Woźniki signals a rapid environmental change to overbank setting like backswamp or crevasse splay, where organic-mediated concentration of phosphorus, released during the reduction of hematite (Ruttenberg & Berner, 1993) could have taken place (cf. Knudsen & Gunter, 2006).

#### *Detrital assemblage: provenance, weathering vs. transportation control*

The small percentage of feldspars, especially albite, in relation to quartz in the non-clay detrital assemblage (Table 1) indicates either a very long

transport or an intense weathering of the parent rock. The detrital origin of kaolinite is evidenced by dominant fragmentation of the kaolinite aggregates. The abundance of kaolinite, and in particular the occasional preservation of very fragile kaolinite vermiform aggregates (Fig. 3g), strongly indicates intense weathering but a short transport. Also, the preservation of kaolinite tridimensional order points to a short transport (Shutov *et al.*, 1970). Since well-ordered kaolinite is uncommon in soils (Wilson, 2013, p. 37), weathering crusts or older, probably Carboniferous sediments are the more plausible sources.

The intensity of weathering can also be assessed from the geochemical data. Retallack (1997) proposed several geochemical parameters, which can be applied to mudstones subjected to pedogenesis. Unfortunately these parameters include K for the calculation of palaeoweathering rate (e.g. Chemical Alteration Index – CAI), and in the studied section potassium was introduced long after deposition. A feasible alternative is the spider diagram, where elements are compared to a reference mudstone composition. For the purpose of this study the Post-Archaean Avarage Shale has been chosen (Taylor & McLennan, 1985, 1995). Enrichment factors ( $F_{el}$ ) have been calculated as follows:  $F_{el} = (C_{el} \text{ sample} / C_{Al} \text{ sample}) / (C_{el} \text{ PAAS} / C_{Al} \text{ PAAS})$ , where  $C_{el}$  – an element concentration, and  $C_{Al}$  – Al concentration (Barbera *et al.*, 2006). The PAAS-standardized distribution curves of selected elements show variable enrichment and depletion trends among all analysed samples (Fig. 15). The most prominent depletion (the concentrations from a few to 100 times smaller than in the PAAS sample) concerns sodium, clearly indicating an intense weathering of the source rocks. Other depletions indicate the lack of organic material (P, Mo), or non-marine conditions (Sr, Ba).

The ratio of kaolinite to 2:1 clays is often interpreted as a climatic signal (e.g. Brański 2011; Lintnerova *et al.*, 2013). On the other hand, it is well established that these minerals are sorted during transportation, because illite and especially illite-smectite particles are much smaller than kaolinite particles (e.g. Ruffell *et al.*, 2002). When the ratio of % kaolinite to % 2:1 clay is plotted against % quartz, used as a proxy for the grain size, a very clear pattern emerges (Fig. 16). Most samples plot as a continuous trend of % kaolinite/% 2:1, increasing with the grain size, which

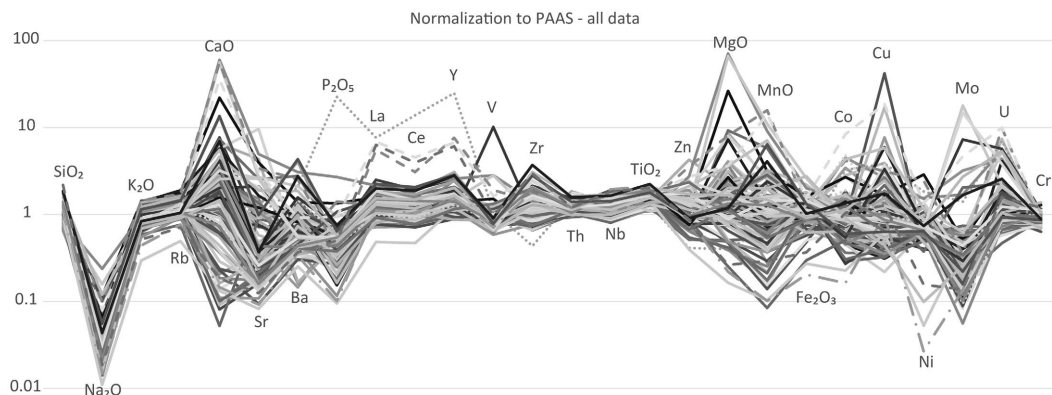


FIG. 15. Spider diagram for selected elements normalized to the composition of the Post-Archean Average Shale (Taylor & McLennan, 1985, 1995). Observe systematic prominent depletion in the sodium content.

indicates that the hydraulic sorting, and not provenance or weathering intensity, is responsible for the observed variation in the mudstone composition. Only one Rhaetian sample has a high kaolinite content and plots clearly off the general trend, implying most probably a change towards more humid climate. This conclusion is supported by the disappearance of hematite at the Norian-Rhaetian border (Table 1). Four other samples with excess kaolinite are dolomitic rocks with a minute admixture of silicates, suggesting possible increased aeolian input.

Potassium feldspar is relatively enriched in the east and chlorite in the west, in rocks of similar quartz content (Table 1). Both minerals are probably detrital, as authigenic textures were not observed. The most feasible explanation for the distribution pattern is the hydraulic sorting control.

The enrichment of hematite in soil horizons documents the weathering origin of hematite and

indicates arid climatic conditions on land, which are consistent with the state of preservation of OM, characterized by intense oxidation in the red clays (Marynowski & Wyszomirski, 2008). Except for the soil horizons, hematite is then a detrital component. Its quantity is controlled also by the post-depositional reduction and, in effect, hematite and pyrite are negatively correlated. The post-depositional reduction of hematite is supported by the oxidized character of OM detected in green interlayers and nests (*sensu* Wyszomirski & Muszyński, 2007). Only in rare levels enriched in terrestrial plant debris OM retains its original, non-oxidized character. Both the TOC content and biomarker distributions are very similar in red clays and green intercalations (Marynowski & Wyszomirski, 2008). These data imply OM oxidation on land under arid conditions and then its transport with hematite and other minerals to the sedimentary basin.

The 060 reflection of 2:1 minerals results from the superposition of the aluminous illitic component, eroded from the older rocks, and a more Fe-rich smectitic weathering product (up to 0.34 Fe/O<sub>10</sub>(OH)<sub>2</sub>). Such Fe-rich smectites are typical soil weathering products (Wilson, 2013, pp. 245–246), thus this composition corroborates the weathering origin of smectite. During diagenetic illitization, this Fe-rich signature of primary smectite is inherited by the illite-smectite (Table 1).

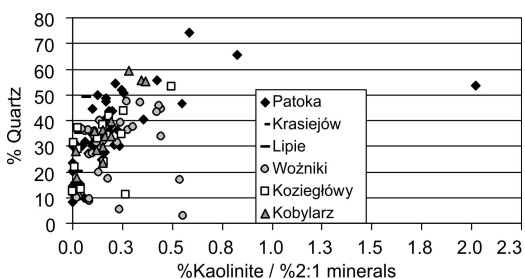


FIG. 16. Smooth evolution of the kaolinite/2:1 minerals ratio with respect to quartz content (proxy for grain size), indicative of hydraulic sorting. Only a Rhaetian sample indicates an increased kaolinite supply.

#### Chemostratigraphic correlation

Chemostratigraphy is a branch of stratigraphy which involves the description and correlation of

sedimentary successions using variations in their elemental composition (Ratcliffe *et al.*, 2010 and references cited therein). The complex post-sedimentary history of the investigated area makes the application of the standard chemostratigraphic approach unfeasible – the distributions of many elements have been affected by the hydrothermal event. Instead, an attempt was made to find chemical signals controlled mostly by provenance, hoping that a gradual change of the source of the detrital material can be detected and used for correlation.

The chemical signal of provenance should be independent from the hydraulic sorting; thus the correlation with % quartz, used as a proxy for the grain size, was checked in the first step. The %  $\text{Al}_2\text{O}_3$  in the investigated rocks is independent of the grain size (Fig. 17), which reflects the higher aluminum concentration in kaolinite, enriched in the coarser grained rocks, with respect to 2:1 clays, enriched in the finer grained rocks (Fig. 3). Thus the elements usually associated with Al: Be, Cr, Ga, Nb, Sc, Ta, and Ti were taken into account. All elements show good positive correlation with Al. For Be, Ga, Sc and Ta the correlations for Patoka and Woźniki wells are very similar, while for Cr, Nb and Ti they differ. The Cr contents in Woźniki depart from the Patoka data contrary to Nb and Ti (Fig. 18). The Cr/Nb and Cr/Ti ratios were then selected as the chemostratigraphic tools.

These indices divide the investigated material into four zones (Table 2, Fig. 19). The top zone I is present only in Patoka, down to 168 m. The zone II involves the bottom of Patoka, Krasiejów, Lipie, top of Woźniki and Koziegłowy, and almost the entire Kobylarz. The zone III was detected in Woźniki, Koziegłowy and at the bottom of Kobylarz, while the zone IV in Woźniki and at the very bottom of Koziegłowy.

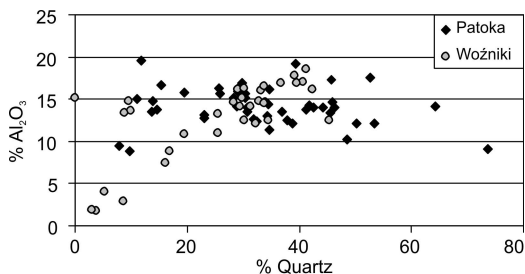


FIG. 17. Stability of aluminium content with respect to grain size, justifying the use of trace elements related to aluminium for chemostratigraphic correlations.

Comparison of the absolute values (Table 2) indicates that Nb and Ti vary much less than Cr; thus the latter is the major controlling factor, which is consistent with the provenance control over these indices. Compared to Ti and Nb, the concentrations of Cr are much more differentiated between the rock types, Cr being indicative of the basic and ultrabasic rocks, where its concentration is up to two orders of magnitude higher than in the acidic rocks (Motzer, 2005). Thus the observed gradual decrease of the two indices up the profiles can be regarded as indicative of decreasing input of the detritus derived from more basic rocks.

The discussed chemical technique seems to be a promising tool for local stratigraphic correlation of the sections poor in index fossils, such as the cases studied here. The results are consistent with lithofacies dating by means of palinostratigraphic data (Orłowska-Zwolińska, 1983; Szulc *et al.*, 2006). However since some diachronism of the chemical indices can be expected, cross-checking by means of e.g. magnetostratigraphy would be required.

## DISCUSSION

The studied Keuper profile is known for scattered occurrences of ore minerals; galena, zinc sulfide,

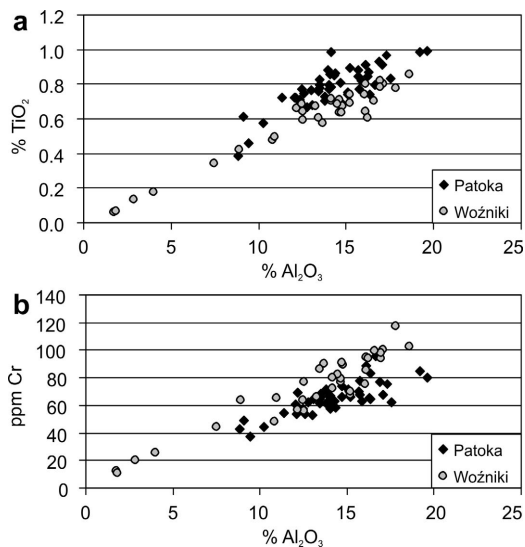


FIG. 18. Correlations of ppm Ti and ppm Cr with %  $\text{Al}_2\text{O}_3$ , characterized by opposite trends with respect to the stratigraphic age (Patoka younger than Woźniki). This pattern justifies the use of Cr/Ti ratio for chemostratigraphy.

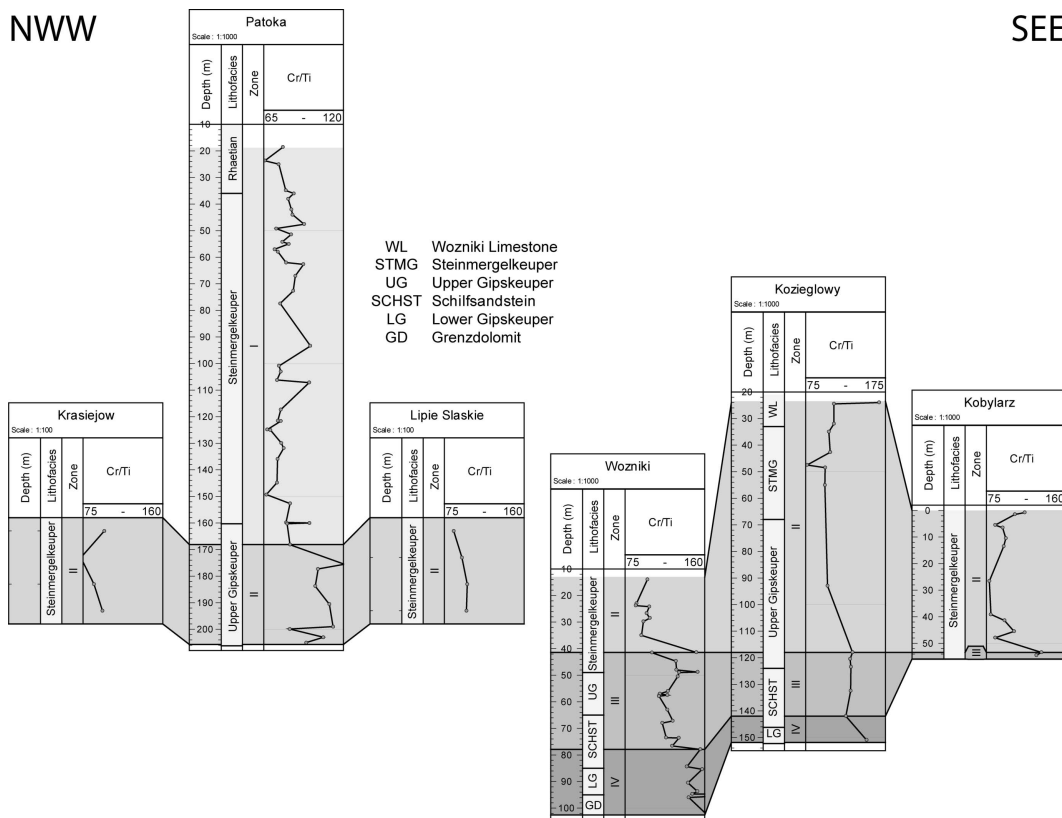


FIG. 19. Chemostratigraphic correlation of the investigated Keuper profiles based on the Cr/Ti ratio. The lithostratigraphic units are given in the second left column of each profile.

bornite, chalcopyrite, azurite and malachite, identified by a microscopic study in the SE part of the study area and farther to SE (Grodzicka-Szymanko, 1993). These data support the interpretation of chemical anomalies presented in this study.

This study confirms earlier data on the mineral composition of the Keuper rocks from the investigated area. Wiewióra & Wyrwicki (1977) studied <math>2 \mu\text{m}</math> fractions and identified illite as the main clay component, illite-smectite with very variable expandability, 20–90%S, Mg-chlorite, goethite, and quartz. Kaolinite was identified only in Steinmergelkeuper, misidentified as Rhaetian in age. Bzowska & Racka (2006) investigated the Krasiejów pit and identified the complete set of minerals described in this study, including palygorskite and hematite, and additionally celestite and baryte. Brański (2011) identified illite, smectite (randomly interstratified IS according to the published XRD pattern), kaolinite, and chlorite,

and observed increasing kaolinite content from Lower Norian to Lower Rhaetian.

In all the Silesian Keuper studies chlorite is reported as a minor component and expandable chlorite or corrensite were not observed. An expandable chlorite as a major component of the Upper Keuper clays has been reported from the Holy Cross Mts. region (Wyszomirski & Muszyński, 2007), located at the depocentre of the Polish part of the Keuper basin (cf. Świdrowska *et al.*, 2008). This regional difference is consistent with the general pattern of clay minerals distribution in the basin (Krum, 1969). Preceding Keuper studies did not recognize illite-smectite and part of illite as products of the Mesozoic thermal event. This finding is applicable to the Keuper rocks from many locations as the Mesozoic thermal events have been very widespread in Europe, at least from the Paris basin to the Upper Silesia (Środoń *et al.*, 2006, and the references therein). In consequence of

this finding, soil smectite was recognized as the primary 2:1 weathering product.

The results of this study offer a warning against a too simplistic use of the kaolinite content as a palaeoclimatic indicator, arguing that most of the observed variation, including the rise of kaolinite content in the Schilfsandstein, can be explained by hydraulic sorting. This interpretation is consistent with the concentration of kaolinite at the edges of the Keuper basin (Krum, 1969). During the wetter Schilfsandstein (Carnian) period kaolinite was not necessarily forming in extra amounts, but the kaolinite available at the basin margin was transported farther into the playa plain. The observed compositional trend indicates that the lack of kaolinite in the central parts of the playa system is a primary sedimentary feature, and not a result of the authigenesis of Mg-clays.

Only the Rhaetian rocks provide evidence of an increased supply of kaolinite, well beyond the hydraulic sorting trend. This anomaly implies a long-term shift towards wetter climate, because it is consistent with the oxygen isotope data presented with other lines of evidence (cf. Feist-Burkhardt *et al.*, 2008), and it is a basin-wide phenomenon (Brański, 2014). In general, an increased supply may also indicate a shift of provenance area, as documented by the contemporary changes in the Nile sediment load (Stanley & Wingerath, 1996). Kaolinite and smectite may form simultaneously by weathering of the same rock in locations with different rainfall (e.g. Barshad, 1966; Johnsson *et al.*, 1993) or may represent subsequent phases of weathering in different climatic conditions.

The depositional environment of the Krasiejów bone bed with palygorskite was identified as a “meandering river of low energy” (Gruszka & Zieliński, 2008) or “typical sheetflood deposits formed by ephemeral stream system under semi-dry climatic conditions”, i.e. evaporite-free sandflat and mudflat sediments succeeding evaporitic playamudflat deposits, which were found in a borehole, ~15 m below the bone bed (Szulc, 2005). Exactly in such position, i.e. at the transition from alluvial fan to mud flats, palygorskite, accompanied by calcrite and gypsum, was found in a Miocene closed basin in Spain (Armenteros *et al.*, 1995) which was never buried to a depth of more than 120 m (Ildefonso Armenteros – personal information). Dolocrete (Ca-dolomite) and silcrete were found farther from the edge zone, in the inner part of mud flats, while sepiolite and magnesian smectite in the depocentre

– saline mud flat/ephemeral lake. The Silesian Keuper facies correspond in this classification to the alluvial fan and the inner mudflat area. The Keuper depocentre deposits (Holy Cross Mts. and many locations in Germany, England, etc.) also contain Mg-clays, but with abundant chloritic components (chlorite, expandable chlorite, and corrensite).

The occurrence of palygorskite in the Krasiejów profile is correlated with a radical increase of gyrogonites frequency, which consists of calcitic remains of the green algae called charophytes (Zatoń *et al.*, 2005). Either both the algae bloom and the palygorskite crystallization are reactions to the same unknown environmental factor, or possibly the cause of palygorskite crystallization was the massive calcite precipitation resulting from algal blooming and the ensuing intense biocalcification. The latter resulted in an increase of the Mg/Ca ratio in the ambient waters, which is a prerequisite for palygorskite formation (cf. Wilson, 2013). Such a concept, assuming the algal-mediated binding of isotopically lighter carbonates, also explains well the exceptionally heavy isotopic composition of carbon from the bone bed calcitic matrix and cements as remnant precipitates.

If the established chemostratigraphic zones are chronostratigraphic, they imply that the playa conditions (Upper Gipskeuper) lasted longer in the Patoka and Kozięgłowy deposits than in more southern locations. This is consistent with the location of the depocentre to the north and with the location of source areas to the S and SE (Gajewska, 1973) in the region undergoing the Cimmerian tectonic uplift since the Ladinian (Szulc, 2000; Paul *et al.*, 2008).

## CONCLUSIONS

Five conclusions have been drawn.

1. The rocks of Silesian Keuper underwent thermal alteration at shallow depth, recorded by the illitization of smectite and by the resetting of fission tracks in apatite. The age of this thermal event was evaluated from AFT as 200–160 Ma, i.e. from Rhaetian to Middle Jurassic, and from K-Ar dating of the clay fractions as  $\leq 164$  Ma. Illite-smectite layer composition established by XRD indicates the maximum temperature of this event close to 125°C, in agreement with the AFT data modelling, which also implies very slow cooling. These age and temperature estimates agree well

with the existing data on the hydrothermal activity in the area, responsible for the formation of Pb-Zn deposits.

2. The assemblage of detrital minerals (quartz, illite, smectite, kaolinite, hematite, minor feldspars and chlorite) documents advanced weathering and transport to the basin from a rather short distance, as indicated by the preservation of kaolinite crystal morphology and structural order. The elevated Fe content of smectite indicates a pedogenic origin, while well-ordered kaolinite is characteristic of the weathering crusts. Most variation in the detrital clay fraction composition is explained by hydraulic sorting, which concentrated kaolinite in coarse-grained rocks, dominant in the marginal facies of the basin, while illite, smectite and chlorite were transported farther towards the centre. Only in the Rhaetian rocks, the high kaolinite content and the disappearance of hematite signal most probably the climatic change.

3. Numerous soil horizons, identified by morphological features (slickensiding, root canals, carbonate concretions, etc.) have been rather short-lasting, as the only detectable mineralogical changes with respect to the underlying sediments, are calcite and hematite accumulations.

4. Authigenic minerals in sediments include calcite, dolomite, Mg-dolomite, palygorskite, pyrite, gypsum, native sulfur and apatite. The oxygen isotopic composition of calcite evolves with time towards lighter values, reflecting stronger influence of rainwater, which can be explained either by the progradation of alluvial fan or the climatic change. Dolomite isotope compositions reflect crystallization from heavier water, not excluding marine incursions. Pyrite, gypsum, native sulfur and apatite signal local organic matter accumulations, which generated reducing conditions and the supply of phosphorus. The environment of palygorskite crystallization is constrained as evolved freshwater by the isotopic composition of coexisting calcite, locally the heaviest but well below the seawater level. Palygorskite formation, specific for the bone-bearing horizon in Krasiejów, is a local episodic phenomenon correlated with a massive algal bloom in ponds located at the transition from mudflats to the alluvial fan, like in other playa systems. The lack of other authigenic Mg-rich clay minerals, typical for the central parts of the playa systems, is consistent with the peripheral location of the investigated area.

5. The Cr/Ti and Cr/Nb ratios in the bulk rocks, diminishing systematically with time, reflect the change in detrital material from more basic to more acidic sources, and allow chemostratigraphic correlation of the investigated profiles.

#### ACKNOWLEDGMENTS

We thank Małgorzata Zielińska for the clay separation work, Tadeusz Kawiak for recording the XRD patterns, Leszek Chudzikiewicz and Andrzej Łaptaś for help with the graphics. The provenance interpretation benefited from the discussions with Mariusz Paszkowski. This work was financed from the NCN project N N307 117037 granted to Prof. Grzegorz Racki, whose help is highly appreciated. The comments of two reviewers and the editorial changes improved significantly the presentation of our study.

#### REFERENCES

- Anczkiewicz A., Środoń J. & Zattin M. (2013) Thermal history of the Podhale basin in the Internal Western Carpathians from the perspective of apatite fission track analyses. *Geologica Carpathica*, **64**, 151–161.
- Armenteros I., Bustillo M.A.A. & Blanco J.A. (1995) Pedogenic and groundwater processes in a closed Miocene basin (northern Spain). *Sedimentary Geology*, **99**, 17–36.
- Barbarand J., Carter A., Wood I. & Hurford T. (2003) Compositional and structural control of fission-track annealing in apatite. *Chemical Geology*, **198**, 107–137.
- Barbera G., Mazzoleni P., Critelli S., Pappalardo A., Lo Giudice A. & Cirrincione R. (2006) Provenance of shales and sedimentary history of the Monte Soro Unit, Sicily. *Periodico di Mineralogia*, **75**, 313–330.
- Barshad I. (1966) The effect of variation in precipitation on the nature of clay mineral formation in soils from acid and basic rocks. *Proceedings of the International Clay Conference*, Jerusalem, **1**, 167–173.
- Botor D., Papiernik B., Mackowski T., Reicher B., Machowski G. & Górecki W. (2012) The thermal history of the Carboniferous source rocks in the Moravian-Silesian Unit, Fore-sudetic Monocline, Poland. *74th EAGE Conference & Exhibition incorporating SPE EUROPEC 2012*, Copenhagen, Denmark, 4–7 June 2012.
- Brański P. (2011) Clay mineral composition in the Triassic and Jurassic deposits from the Polish Basin – a record of palaeoclimatic and palaeoenvironmental changes. *Biuletyn Państwowego Instytutu Geologicznego*, **444**, 15–32 (in Polish).
- Brański P. (2014) Climatic disaster at the Triassic-

- Jurassic boundary – a clay minerals and major elements record from the Polish Basin. *Geological Quarterly*, **58** (in press, doi: 10.7306/gq.1161)
- Braun J., Van der Beek P. & Batt G. (2008) *Quantitative Thermochronology*. Cambridge University Press.
- Brindley G.W. & Brown G. (1980) *Crystal Structures of Clay Minerals and their X-ray Identification*. Mineralogical Society Monograph No. 5, London.
- Bzowska G. & Racka M. (2006) Kajper Krasiejowa okiem geochemika i mineraloga. *Gospodarka Surowcami Mineralnymi*, **22**, zeszyt specjalny 3, 355–358.
- Chaffee M.A., Eppinger R.G., Lason K., Slosarz J. & Podemski M. (1994) The Myszków porphyry copper-molybdenum deposit, Poland. *International Geology Review*, **36**, 947–960.
- Deczkowski Z. (1977) Geology of the Permo-Mesozoic cover and its basement in the eastern part of the fore-Sudetic monocline (Kalisz-Częstochowa area). *Prace Instytutu Geologicznego*, **82**, 63 pp.
- Donelick R.A., Sullivan P.B. & Ketcham R.A. (2005) Apatite fission-track analysis. *Revue of Mineralogy and Geochemistry*, **58**, 49–94.
- Dunkl I. (2002) TRACKKEY: A Windows program for calculation and graphical presentation of fission track data. *Computer Geoscience*, **28**, 3–12.
- Dzik J., Sulej T., Kaim A. & Niedźwiedzki R. (2000) Późnotriasowe cmentarzysko kręgowców śladowych w Krasiejowie na Śląsku Opolskim. *Przegląd Geologiczny*, **48**, 226–235.
- Feist-Burkhardt S., Götz A., Szulc J., Borkhataria R., Geluk M., Haas J., Hornung J., Jordan P., Kempf G., Michalík J., Nawrocki J., Reinhardt L., Ricken W., Röhlh H. G., Ruffer T., Török Á. & Zühlke R. (2008) Triassic. Pp. 1–73 in: *The Geology of Central Europe, 2. Mesozoic and Cenozoic* (T. McCann, editor). The Geological Society of London.
- Gajewska I. (1997) Charakterystyka osadów piaskowca trzcinowego na Niziu Polskim. *Kwartalnik Geologiczny*, **17**, 507–515.
- Galbraith R.F. (1981) On statistical models for fission track counts. *Mathematical Geology*, **13**, 471–438.
- Galbraith R.F. (1990) The radial plot; graphical assessment of spread in ages. *Nuclear Tracks and Radiation Measurements*, **17**, 207–214.
- Galbraith R.F. & Laslett G.M. (1993) Statistical models for mixed fission track ages. *Nuclear Tracks and Radiation Measurements*, **21**, 459–470.
- Green P.F. (1981) A new look at statistics in fission-track dating. *Nuclear Tracks*, **5**, 77–86.
- Grodzicka-Szymanko W. (1993) Trias górny. *Prace Instytutu Geologicznego*, **83**, 105–111.
- Gruszka B. & Zieliński T. (2008) Evidence for a very low-energy fluvial system: a case study from the dinosaur-bearing Upper Triassic rocks of Southern Poland. *Geological Quarterly*, **52**, 239–252.
- Heijlen W., Muechz P., Banks D.A., Schneider J., Kucha H. & Keppens E. (2003) Carbonate-hosted Zn-Pb deposits in Upper Silesia, Poland: Origin and evolution of mineralizing fluids and constraints on genetic models. *Economic Geology*, **98**, 911–932.
- Heuser M., Andrieux P., Petit S. & Stanjek H. (2013) Iron-bearing smectites: a revised relationship between structural Fe, *b* cell edge lengths and refractive indices. *Clay Minerals*, **48**, 97–103.
- Jackson M.L. (1975) *Soil Chemical Analysis – Advanced Course*. Published by the author, Madison, Wisconsin.
- Jarvis I. & Jarvis K.E. (1992) Inductively coupled plasma-atomic emission spectrometry in exploration geochemistry. Pp. 22–56 in: *Analytical Methods in Geochemical Exploration* (G.E.M. Hall & B. Vaughlin, editors). Journal of Geochemical Exploration Special Issue.
- Jans C.V. (2006) Clay mineralogy of the Permo-Triassic strata of the British Isles: onshore and offshore. *Clay Minerals*, **41**, 309–354.
- Jans C.V., Mitchell J.G., Scherer M. & Fisher M.J. (1994) Origin of Permo-Triassic clay mica assemblage. *Clay Minerals*, **29**, 575–589.
- Jans C.V., Fisher M.J. & Merriman R.J. (2005) Origin of the clay mineral assemblages in the Germanic facies of the English Trias: application of the spore colour index method. *Clay Minerals*, **40**, 115–129.
- Johnsson M.J., Ellen S.D. & McKittrick M.A. (1993) Intensity and duration of chemical weathering: an example from soil clays of the southeastern Koolau Mountains, Oahu, Hawaii. *Geological Society of America Special Paper*, **284**, 147–170.
- Ketcham R.A. (2005) Forward and inverse modeling of low-temperature thermochronometry data. Pp. 275–314 in: *Low-Temperature Thermochronology: Techniques, Interpretations, and Applications* (P.W. Reiners & T.A. Ehlers, editors). *Review in Mineralogy and Geochemistry*, **58**, Mineralogical Society of America, Washington DC.
- Ketcham R.A., Carter A., Donelick R.A., Barbarand J. & Hurford A.J. (2007) Improved modeling of fission-track annealing in apatite. *American Mineralogist*, **92**, 799–810.
- Knudsen A.C. & Gunter M.E. (2006) Sedimentary phosphorites – an example: Phosphoria Formation, southeastern Idaho, U.S.A. Pp. 363–389 in: *Phosphates: Geochemical, Geobiological, and Materials Importance* (M.J. Kohn, J. Rakovan & J.M. Hughes, editors). *Reviews in Mineralogy and Geochemistry*, **48**, Mineralogical Society of America, Washington, DC.
- Kozłowski A. (1995) Origin of Zn-Pb ores in the Olkusz and Chrzanów districts: a model based on fluid inclusions. *Acta Geologica Polonica*, **45**, 83–141.
- Kozłowski A. & Górecka E. (1993) Sphalerite origin in the Olkusz mining district: a fluid inclusion model. *Geological Quarterly*, **37**, 291–306.

- Krum H. (1969) A scheme of clay mineral stability in sediments, based on clay mineral distribution in Triassic sediments of Europe. *Proceedings of the International Clay Conference*, Tokyo, 313–324.
- Lintnerová O., Michalik J., Uhlík P. & Soták J. (2013) Latest Triassic climate humidification and kaolinite formation (Western Carpathians, Tatric Unit of the Tatra Mts.). *Geological Quarterly*, **57**, 701–728.
- Lippman F. (1956) Clay minerals from the Röt member of the Triassic near Göttingen, Germany. *Journal of Sedimentary Petrology*, **26**, 125–139.
- Marek S. & Pajchlowa M. (1997) The epicontinental Permian and Mesozoic in Poland. *Prace Polskiego Instytutu Geologicznego*, **153**, 452 pp.
- Marynowski L. & Wyszomirski P. (2008) Organic geochemical evidences of early diagenetic oxidation of the terrestrial organic matter during the Triassic arid and semi arid climatic conditions. *Applied Geochemistry*, **23**, 2612–2618.
- Marynowski L., Zatoń M., Rakociński M., Filipiak P., Kurkiewicz S. & Pearce T.J. (2012) Deciphering the upper Famennian Hangenberg Black Shale depositional environments based on multi-proxy record. *Palaeogeography, Palaeoclimatology, Palaeoecology*, **346/347**, 66–86.
- Motzer W.E. (2005) Chemistry, geochemistry, and geology of chromium and chromium compounds. Pp. 23–91 in: *Chromium (VI) Handbook* (J. Guertin, J.A. Jacobs, & C.P. Avakian, editors), CRC Press, USA.
- Orłowska-Zwolińska T. (1983) Palinostratygrafia epikontynentalnych osadów wyższego triasu w Polsce. *Prace Instytutu Geologicznego*, **104**, 1–89.
- Pan Y. & Fleet M.E. (2002) Compositions of the apatite-group minerals: substitution mechanisms and controlling factors. Pp. 13–49 in: *Phosphates: Geochemical, Geobiological, and Materials Importance* (M.J.Kohn, J. Rakovan & J.M. Hughes, editors). *Reviews in Mineralogy and Geochemistry*, **48**, Mineralogical Society of America, Washington, DC.
- Paul J., Wemmer K. & Ahrendt H. (2008) Provenance of siliciclastic sediments (Permian to Jurassic) in the Central European Basin. *Zeitschrift der Deutschen Gesellschaft für Geowissenschaften*, **159**, 641–650.
- Peters K.E., Walters C.C. & Moldowan, J.M. (2005) *The Biomarker Guide*. Vol. 2, Cambridge University Press, 1155 pp.
- Ratcliffe K.T., Wright A.M. & Schmidt K. (2012) Application of inorganic whole-rock geochemistry to shale resource plays: an example from the Eagle Ford Shale Formation, Texas. *The Sedimentary Record*, **10**, 4–9.
- Reinhardt L. & Ricken W. (2000) The stratigraphic and geochemical record of Playa Cycles: monitoring a Pangaeon monsoon-like system (Triassic, Middle Keuper, S. Germany). *Palaeogeography, Palaeoclimatology, Palaeoecology*, **161**, 205–227.
- Retallack G. (1997) *A Color Guide to Paleosols*. John Wiley & Sons, Chichester.
- Ruffell A., McKinley J.M. & Worden R.H. (2002) Comparison of clay mineral stratigraphy to other proxy paleoclimate indicators in the Mesozoic of NW Europe. *Philosophical Transactions of the Royal Society of London*, **A360**, 675–693.
- Ruttenberg K.C. & Berner R.A. (1993) Authigenic apatite formation and burial in sediments from non-upwelling continental margin environments. *Geochimica et Cosmochimica Acta*, **57**, 991–1007.
- Shaw D.M. (1968) A review of K-Rb fractionation trends by covariance analysis. *Geochimica et Cosmochimica Acta*, **32**, 573–601.
- Shutov V.D., Aleksandrova A.V. & Losievskaya S.A. (1970) Genetic interpretation of the polymorphism of the kaolinite group in sedimentary rocks. *Sedimentology*, **15**, 69–82.
- Środoń J. (1981) X-ray identification of randomly interstratified illite/smectite in mixtures with discrete illite. *Clay Minerals*, **16**, 297–304.
- Środoń J. (1984) X-ray powder diffraction identification of illitic materials. *Clays and Clay Minerals*, **32**, 337–349.
- Środoń J. (2007) Illitization of smectite and history of sedimentary basins. *Proceedings of the 11<sup>th</sup> EUROCLAY Conference*, Aveiro, Portugal, 74–82.
- Środoń J. (2010) Evolution of boron and nitrogen content during illitization of bentonites. *Clays and Clay Minerals*, **58**, 743–756.
- Środoń J. & Kawiak T. (2012) Mineral compositional trends, petrophysical and well logging parameters, and the composition of pore water in clastic rocks from shallow burial (Miocene of the Carpathian Foredeep, SE Poland) revealed by QUANTA+BESTMIN analysis. *Clays and Clay Minerals*, **60**, 63–75.
- Środoń J. & McCarty D.K. (2008) Surface area and layer charge of smectite from CEC and EGME/H<sub>2</sub>O retention measurements. *Clays and Clay Minerals*, **56**, 155–174.
- Środoń J. & Paszkowski M. (2011) Role of clays in diagenetic history of boron and nitrogen in the Carboniferous of Donbas (Ukraine). *Clay Minerals*, **46**, 561–582.
- Środoń J., Drits V.A., McCarty D.K., Hsieh J.C.C. & Eberl D.D. (2001) Quantitative XRD analysis of clay-rich rocks from random preparations. *Clays and Clay Minerals*, **49**, 514–528.
- Środoń J., Clauer N., Banaś M. & Wójtowicz A. (2006) K-Ar evidence for a Mesozoic thermal event superimposed on burial diagenesis of the Upper Silesia Coal Basin. *Clay Minerals*, **41**, 671–692.
- Środoń J., Zeelmaekers E. & Derkowski A. (2009) The charge of component layers of illite-smectite in bentonites and the nature of end-member illite. *Clays*

- and *Clay Minerals*, **57**, 649–671.
- Środoń J., Drygant D.M., Anczkiewicz A.A. & Banaś M. (2013) Thermal history of the Silurian in the Podolia segment of the SW margin of the East European Craton inferred from combined XRD, K-Ar, and AFT data. *Clays and Clay Minerals*, **61**, 107–132.
- Stanley D.J. & Wingerath J.G. (1996) Nile sediment dispersal altered by the Aswan High Dam: the kaolinite trace. *Marine Geology*, **133**, 1–9.
- Suggate R.P. (1998) Relations between depth of burial, vitrinite reflectance and geothermal gradient. *Journal of Petroleum Geology*, **21**, 5–32.
- Sweeney J.J. & Burnham A.K. (1990) Evaluation of a simple model of vitrinite reflectance based on chemical kinetics. *The American Association of Petroleum Geologists Bulletin*, **74**, 1559–1570.
- Świdrowska J., Hakenberg M., Poluhtovič B., Seghedi A. & Višňakov I. (2008) Evolution of the Mesozoic basins on the southwestern edge of the East European Craton (Poland, Ukraine, Moldova, Romania). *Studia Geologica Polonica*, **130**, 3–130.
- Szulc J. (2000) Middle Triassic evolution of the northern peri-Tethys area as influenced by early opening of the Tethys ocean. *Annales Societatis Geologorum Poloniae*, **70**, 1–48.
- Szulc J. (2005) Sedimentary environments of the vertebrate-bearing Norian deposits from Krasiejów, Upper Silesia (Poland). *Halleschs Jahrbuch für Geowissenschaften*, **B19**, 161–170.
- Szulc J. & Racki G. (2014) Formacja grabowska – podstawowa jednostka litostratygraficzna kajpru Górnego Śląska. *Przegląd Geologiczny*, **62**, (in print).
- Szulc J., Gradziński M., Lewandowska A. & Heunisch C. (2006) The Upper Triassic crenogenic limestones in Upper Silesia (southern Poland) and their paleoenvironmental context. *Geological Society of America Special Paper*, **416**, 133–151.
- Taylor S.R. & McLennan S.M. (1985) *The Continental Crust: Its Composition and Evolution*. Blackwell Scientific.
- Taylor S.R. & McLennan S.M. (1995) The geochemical evolution of the continental crust. *Reviews of Geophysics*, **33**, 241–265.
- Tari G., Poprawa P. & Krzywiec P. (2012) Silurian lithofacies and paleogeography in Central and Eastern Europe: implications for shale gas exploration. *SPE 151606*, 1–11.
- Veizer J., Bruckschen P., Pawelleka F., Diener A., Podlaha O.G., Carden G.A.F., Jasper T., Korte C., Strauss H., Azmy K. & Ala D. (1997) Oxygen isotope evolution of Phanerozoic seawater. *Palaeogeography, Palaeoclimatology, Palaeoecology*, **132**, 159–172.
- Wagner G., & Van den Haute P. (1992) *Fission-Track Dating*. Kluwer Acad., Dordrecht, 285 pp.
- Wiewióra A. & Wyrwicki R. (1977) Minerality ilaste triasu górnego okolic Kluczborka. *Geological Quarterly*, **21**, 269–278.
- Williams L., Środoń J., Huff W., Clauer N. & Hervig R. (2013) Light element distributions (N, B, Li) in Baltic Basin bentonites record organic sources. *Geochimica et Cosmochimica Acta*, **120**, 582–599.
- Wilson M.J. (2013) *Sheet Silicates: Clay Minerals*. The Geological Society, London, 724 pp.
- Worden R.H. (2006) Dawsonite cement in the Triassic Lam Formation, Shabwa Basin, Yemen: A natural analogue for a potential mineral product of subsurface CO<sub>2</sub> storage for greenhouse gas reduction. *Marine and Petroleum Geology*, **23**, 61–77.
- Wyszomirski P. & Muszyński M. (2007) Charakterystyka mineralogiczno-surowcowa przerostów i wtrąceń w czerwonych kopalinach ilastych triasu północnego obrzeżenia Gór Świętokrzyskich. *Gospodarka Surowcami Mineralnymi*, **23**, 5–28.
- Zatoń M., Piechota A. & Sienkiewicz E. (2005) Late Triassic charophytes around bone-bearing bed at Krasiejów (SW Poland) – palaeoecological and environmental remarks. *Acta Geologica Polonica*, **55**, 283–293.
- Ziegler P.A. (1990) *Geological Atlas of Western and Central Europe*. Shell Internationale Petroleum Maatschappij, The Hague.